Recommendation for strut designs of vertical axis wind turbines: Effects of strut profiles and connecting configurations on the aerodynamic performance

Weipao Miao[a], Qingsong Liu[a], Qiang Zhang[a], Zifei Xu[a,b], Chun Li[a,c,*], Minnan Yue[a], Wanfu Zhang[a], Zhou Ye[a]

[a] *School of Energy and Power Engineering, University of Shanghai for Science and Technology, Shanghai, 200093. China*

[b] *Department of Maritime and Mechanical Engineering, Liverpool John Moores University, Liverpool, Byrom Street, L3 3AF, UK*

[c] *Shanghai Key Laboratory of Multiphase Flow and Heat Transfer in Power Engineering, Shanghai 200093, China*

Abstract: The strut is a necessary support structure that connects the vertical axis wind turbine blade to the rotating shaft and transfers the torque, and is one of the key factors affecting the aerodynamic performance of the wind turbine. However, research on struts is limited and the appropriate strut design remain uncertain. Therefore, in this paper, the struts of a straight-bladed vertical axis wind turbine are investigated by a three-dimensional computational fluid dynamics approach, to find the appropriate strut design parameters that minimize the impact on the aerodynamic performance. Thirty strut profiles with different chord lengths, thicknesses, areas, and streamlined shapes were parametrically created and analyzed, including a novel strut-specific profile proposed in this paper. Furthermore, all strut connecting parameters, such as spanwise and chordwise positions, connecting angle and fairing were investigated. The results show that the power loss of a vertical axis wind turbine has a relatively linear relationship with the dimensionless absolute thickness of the strut within a certain range. The strut chord length is another important influencing factor. Equal chord lengths of the strut and the blade should be avoided as much as possible. The proposed novel olivary strut profile has lower drag characteristics and more favorable geometrical structural properties compared to the most used NACA airfoil. The influence of the spanwise connecting position (within the range around the blade quarter span) is minor. But the chordwise position has a significant effect, and special attention should be paid to avoid the strut maximum thickness position connecting with the blade aerodynamic center, which will result in the greatest performance degradation. Analysis of the connecting angles shows that inclined struts are suitable for small wind turbines. The fairing is effective when the strut chord length is equal to or longer than the blade chord length. With these results, a set of recommended design parameters for vertical axis wind turbine struts is presented.

Key words: *Strut Effects; H-type VAWT; Aerodynamic Drags; Strut Parameters; CFD;*

Nomenclature

A_B	Cross-sectional Area of Blade [m$^{2]}$	LE	Leading Edge [-]
AC	Aerodynamic Center [-]	MTP	Maximum Thickness Position [-]
ARC	Asymptotic Range of Convergence [-]	M_y	Bending Moment [N·m]
A_S	Cross-sectional Area of Strut [m^2]	N	Number of Blades [-]
c	Chord Length [m]	N_k	Number of Grids [-]
CAD	Computer Aided Design [-]	P	Power Output [W]
c_B	Chord Length of Blade [m]	R	Rotor Radius [m]
CFD	Computational Fluid Dynamic [-]	RANS	Reynolds-Averaged Navier-Stokes [-]
COE	Cost of Electricity [-]	Re	Reynolds Number [-]
C_P	Power Coefficient [-]	S	Strut Position [-]
C_{Pre}	Pressure Coefficient [-]	SIMPLE	Semi-Implicit Method for Pressure Linked Equations [-]
C_Q	Torque Coefficient [-]	SST	Shear Stress Transport [-]
c_S	Chord Length of Strut [m]	t	Time [s]
D	Rotation Diameter [m]	T_{abs}	Strut Absolute Thickness [-]
d_{LE}	Distance Between Strut LE and Blade LE [m]	TCR	Thickness-Chord Ratio [-]
d_{MTP}	Distance Between Strut MTP and Blade LE [m]	TSR λ	Tip Speed Ratio [-]
D_T	Tower Diamater [m]	V_∞	Incoming Velocity [m/s]
F_D	Drag Force [N]	VAWTs	Vertical Axis Wind Turbines [-]
F_L	Lift Force [N]	W	Synthetic Velocity [m/s]
F_N	Normal Force [N]	α	Angle of Attack [-]
F_T	Tangential Force [N]	β	Fixed Pitch Angle [°]
GCI	Grid Convergence Index [-]	ζ	Strut Connecting Angle [°]
H	Blade Height [m]	θ	Azimuth Angle [°]
AC	Aerodynamic Center [-]	θ_S	Tangent Angle of Strut Profile Edge [°]
ARC	Asymptotic Range of Convergence [-]	μ	Dynamic Viscosity [Pa·s]
h	Half Height of Blade [m]	ρ	Air Density [kg/m^3]
HAWTs	Horizontal Axis Wind Turbines [-]	σ	Solidity of Rotor [-]
IDDES	Improved Detached Eddy Simulation [-]	σ_S	Stress [Pa]
I_x	Moment of Inertia [m^4]	Ω	Rotational Speed [rad/s]

* Corresponding author. Tel, +021-55271729
E-mail address: linchun_usst@163.com

1. Introduction

Wind energy is clean and renewable, with considerable potential to alleviate the future fossil fuel scarcity and price increase[1]. Through years of development, horizontal axis wind turbines (HAWTs) are the dominant wind energy utilization devices on the market today[2]. However, recent studies reveal that it is difficult to further reduce the cost of electricity (COE) by increasing the size of HAWTs[3-5]. In addition, for the current global emphasis on offshore wind energy, HAWTs have to invest more in the construction and subsequent operation and maintenance of offshore floating platforms due to their high center of gravity[5]. As these issues of HAWTs became more prominent, attention is once again being focused on vertical axis wind turbines (VAWTs), especially the lift-type VAWT with efficiency comparable to those of HAWTs[6, 7]. VAWTs have no yaw system, low center of gravity, segmental blades, less deformation and edgewise loading, which is more favorable to design as floating type, and their mooring system cost can be reduced by more than 20% compared with HAWTs[8, 9]. These advantages make VAWTs potentially more suitable than HAWTs as the future offshore wind energy. Many countries have made VAWTs a research priority, leading to their commercialization[7].

However, as the development of VAWTs has lagged behind that of HAWTs in the last few decades, resulting in the technological maturity of VAWTs still facing challenges[10]. In particular, despite the evident advantages of VAWTs, optimal aerodynamic design is still a prominent issue[11]. As an example, Fig. 1 shows the design parameters that affect the aerodynamic performance of a straight-bladed VAWT, including blade tip design[12, 13], pitch angle[14], coning angle[15], solidity[16], blade aspect ratio[17], airfoil[18, 19], blade orientation[20], wind turbine height-to-radius ratio[21], tower[22] and strut[23], etc. Many of these factors are also interrelated and thus affect the overall power efficiency. A detailed review of these parameters is presented by Hand et al.[24]. Fortunately, with the rapid development of wind turbine technology, considerable studies on VAWTs are being carried out by academics around the world in an endeavor to provide optimum design solutions for VAWTs. In addition, many studies have attempted to improve the aerodynamic performance of the VAWT in terms of flow control methods, such as the active flow control using suction[25, 26], blowing[27], dynamics flap[28] and variable pitch[29], or the passive flow control by means of adaptive flap[30], Gurney flap[31], deflector[32], leading edge serrations[33], slotted airfoil blades[34], or dual blades[35, 36].

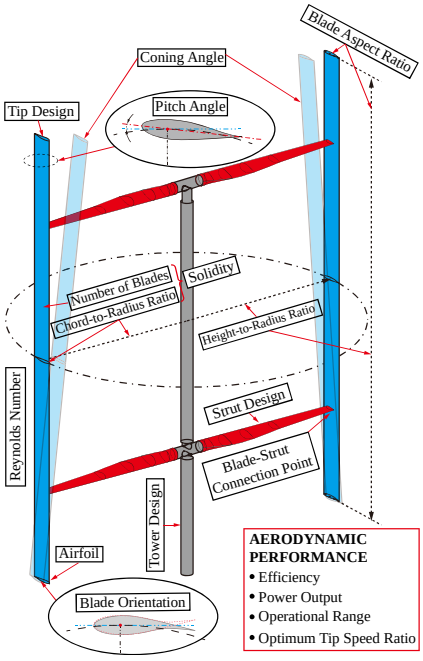

Fig. 1. Design parameters affecting the aerodynamic performance of the VAWT[24].

It is important to noted that most of the past VAWT performance studies are investigated through two-dimensional (2D) models[28, 37, 38] due to the limitations in computer technology and resources. When three-

dimensional (3D) models are used, the aerodynamic performance of most optimally designed VAWTs will be substantially lower than that of the 2D models. In addition to the blade tip loss effect[12] of 3D blades, the strut effect of VAWTs is another important factor. However, the current limited strut studies are not sufficient to provide suitable design parameters, and further investigation is needed. This is the primary research objective of this paper.

1.1. Strut Effect of VAWTs

Currently, lift-type VAWTs that have been validated as efficient and feasible by extensive research include: the straight-blade "Musgrove H-rotor", the helical-blade "Gorlov" and the curved-blade "Darrieus *Φ*-rotor"[39].

The strut (also called support structures or arms) is an essential generic structure for a VAWT. For the helical and straight blade VAWTs, the struts not only provide structural support to resist aerodynamic, gravitational, and inertial loads on the blade, but are also responsible for transferring torque to the shaft for power generation and strongly influence the natural frequency of the rotor[40, 41]. For the Φ-type wind turbine, although the 34 m VAWT first developed by Sandia Labs stabilized the curved blade by its tension without the need for struts, they emphasized the necessity of using struts for reinforcement due to the increasing weight of the large-scale VAWT blades[11]. Consequently, despite their different types, all three VAWTs invariably require struts to provide the necessary structural connection and support, especially for large-scale VAWTs.

However, the presence of struts generates two types of drag during the turbine rotation: the direct profile drag caused by the struts cross-sectional shape and the induced drag due to the interference at the strut-blade connecting interface[11],[42]. Many studies have demonstrated that both types of drag significantly reduce the VAWT power output. Tests by SANDIA showed that the struts reduced the maximum power output of the VAWT by 26%[43]. An experimental study by Li et al.[44] showed that the output power of the VAWT with struts measured with a torque meter and a six-component balance was significantly lower than the power measured with the pressure taps on the blade surface. Recent numerical simulations by Aya et al.[23, 45] also showed that at high tip-speed-ratio (TSR), the struts reduced the power of their 12 kW H-type VAWT by 43%. This significant degradation in aerodynamic performance is due to the faster rotor speed at high TSR, resulting in an exponential increase in the strut effect[14]. Therefore, due to the pronounced influence of the strut, any attempt to model the VAWT without modelling struts will lead to inaccurate solutions.

1.2. Influences of Strut Parameters

It is clear that a reasonable strut design is essential to reduce the power loss of VAWT. However, the design parameters of the strut are numerous, and the related research is still limited. The following four sections involve the overview of different strut parameters.

1.2.1. Strut Profiles

According to fundamental aerodynamic principles, it is known that the cross-sectional profile shape plays a dominant role in the drag characteristics of the strut. Early VAWTs use cylindrical strut profiles, considering only the support function[14]. The drag effect of cylinder struts proved to be extremely significant. Peter et al. [46] compared the drag of a NACA 0021 airfoil and a cylinder strut using a hydraulic tow tank. They rotated the struts individually to measure their drag characteristics and found that the high drag produced by the cylinder strut prevented the turbine from producing power output, while the power losses of the NACA airfoil strut were much lower. Apparently, the streamlined cross section reduces the profile drag of the strut itself. For this reason, Mazharul et al.[41],[47] designed a special profile for the strut named MI-Struct1, and they confirmed through their in house code that the profile drag of MI-Struct1 is lower than that of the E862 airfoil.

However, it is not enough to only focus on the strut profile drag. The strut-to-blade connection type also affects the aerodynamic performance of the blade itself, known as the induced drag. Philip et al. [48] experimentally evaluated the effect of two types of strut-to-blade connections on the power efficiency of a vertical axis tidal turbine bolted flat strut and a fused NACA0012 profiles strut. Their results showed a 50% decrease in efficiency

for the turbine with flat struts. Unfortunately, it is difficult to isolate in the experiment whether profile or induced drag has a stronger effect. But at least their combined effect on the turbine performance is significant. Yutaka et al. [49] compared the effect of three strut profiles, NACA 0018 airfoil, rectangular and circular, of the same thickness on the resistance torque (the direct drag) and the tangential torque (the induced drag). They decomposed these two types of torque to the differential pressure and frictional drags, and found that the effect of struts on the blade frictional drag was much smaller. Another interesting finding was that the profile drag was higher than the induced drag for the rectangular and circular struts, while the opposite was true for NACA airfoil. Unfortunately, they did not further investigate the flow mechanism responsible for this phenomenon.

These previous studies analyzed the effect of different strut profiles with the same chord length or the same thickness, but another important factor was not sufficiently considered. That is, the structural strength of these struts is different, which leads to unfair comparisons in many studies. The design of struts involves a compromise between aerodynamic performance and structural strength[50]. Mojtabadeng et al.[40] considered this factor and compared different strut profiles such as airfoil, cylinder, circular, rectangular and diamond with the same cross-sectional area. The total power loss and structural stresses of different struts were analyzed by their in-house program. The results show that the drag of rectangular and diamond profiles is greater than that of circular profile, and the streamlined airfoil profile is obviously the best choice. Unfortunately, however, their analysis is unable to identify the effect of strut profile on the blade aerodynamic performance (the induced drag).

1.2.2. Strut Connecting Position

The connecting position of the strut could be discussed in two aspects, the spanwise and the chordwise.

(i) The Spanwise Position

To balance the rotor, all types of struts generally installed symmetrically to the central height position of the blade. Depending on the spanwise connecting position, the VAWT struts are classified into the three types illustrated in Fig. 2, the middle span, the quarter span, and the end span. Noted that the quarter span in Fig. 2 (b) is not fixed at the 1/4 position of the blade exactly, but at the position between the middle span and the end span.

Intuitively, the middle span should have the least drag because it uses one strut on each blade[51]. Nevertheless, the results of Philip et al.[48] and Thierry et al.[51] showed that the end span installed struts have higher VAWT aerodynamic efficiency. This is because the middle or quarter span struts interrupt the high-performance region of the blade surface. On the contrary, the end span installed struts do not interfere with the blade, but also contribute to reducing the blade tip losses because it acts like an endplate[51].

However, the installation of struts should consider not only the aerodynamic performance but also the necessary structural support, which is even more important for large-scale VAWTs. If only one strut is used for each blade, the aerodynamic forces and the gravity of the blade will generate significant bending stresses at the joints. Mojtaba et al.[40] analyzed and optimized the blade bending stresses for these three strut spanwise positions, and showed that the maximum stresses for the blade with end span struts were nearly five times higher than those for the blade with quarter span struts. This was also confirmed by Hameed et al.[52] through finite element analysis. Therefore, despite the relatively better aerodynamic performance of the end span struts, the structural risk is significantly higher. On the contrary, the quarter span strut is more balanced in terms of aerodynamic and structural performance and is a relatively better choice[24]. In addition, blades with quarter span struts can also reduce the tip loss through a blade tip design[12], thus achieving similar results as end span struts, but with better structural properties.

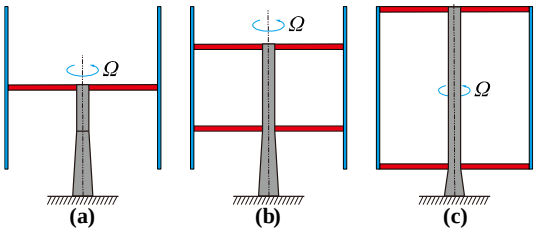

Fig. 2. VAWTs with different strut spanwise connecting positions[50]. Ω is the rotating speed. (a) Middle Span. (b) Quarter Span. (c) End Span.

(ii) The Chordwise Position

In VAWT fabrication, the struts are connected at the mid-chord position (i.e., 0.5c) of the blade in most cases[53]. However, Bianchini et al. [54] showed that since the aerodynamic center (AC) of most subsonic airfoils is located at 0.25c, the actual force on the blade will change when the connecting position is located at 0.5c as shown in Fig. 3 (a). This is equivalent to a slight increase in the blade radius and an additional pitch angle, which also causes a pitching moment.to be generated by the normal component force of the blade. This phenomenon is more pronounced in smaller wind turbines with a higher solidity. Therefore, they recommend a chordwise connecting position of 0.25c for the struts.

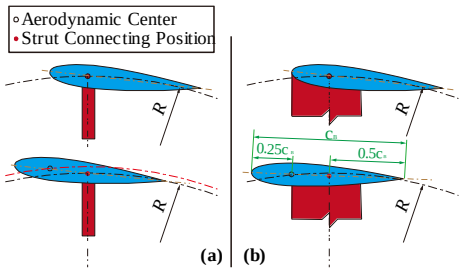

Fig. 3. Different strut chordwise connecting positions for various strut chords. (a) ACs on different radius. (b) ACs on the same radius. c_B represents the blade chord. R is the rotor radius.

However, since the 2D VAWT numerical model[53, 54] used in previous studies on the blade-strut chordwise connection could not practically include struts, what they actually analyzed was the variation of the rotor radius and the blade pitch angle due to different connection positions. For the 3D VAWT model, another important factor, the strut width, must be considered when analyzing the spanwise connecting position, as shown in Fig. 3 (b). In the case where the strut chord length is smaller than the blade chord, for blades with AC on the same radius, the variation of the strut chordwise position does not affect the AC location and the pitch angle, but affects the flow on the blade surface resulting in different induced drags. Research on this subject has not been carried out so far.

1.2.3. Strut Connecting Angles

In addition to the common horizontal installation, the strut can be inclined at a certain angle, as shown in Fig. 4. For a straight-bladed VAWT, the advantage of using inclined struts is that the tower height and the center of gravity of the rotor can be reduced[11], even to the bottom, as shown in Fig. 4 (c). Many concept designs of large-scale offshore VAWTs[7, 55] have adopted this V-rotor because its low center of gravity characteristic is beneficial for the stability of floating platforms. Agostino et al. [56] proposed a combined horizontal and inclined VAWT strut, and their numerical simulations and experimental results showed that the inclined part of the strut could captures additional wind energy and compensate for its own drag. Thierry et al. [51] also found that the inclined 45° strut provide positive moment when analyzing the inclined angle of the strut mounted on the end span, but it significantly interfered with the blade aerodynamic efficiency. Since their struts extended from the blade tip, it is actually more like the effect of different blade tip designs.

It should be noted that the non-vertical connection of the inclined strut to the blade will result in bending moment, rather than pure compression and tension as in the case of horizontal struts[57]. Therefore, for structural reasons, Hand et al. [24] suggested a horizontal form of strut for large-scale VAWTs. Nevertheless, a comparison of

the effects of horizontal and inclined struts on the VAWT aerodynamic performance is still lacking.

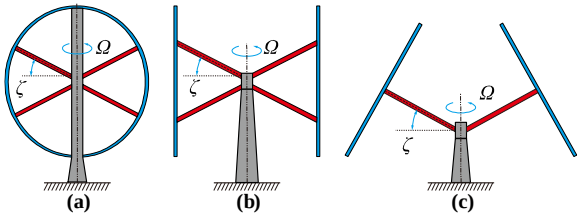

Fig. 4. VAWTs with inclined struts. ξ is the inclined angle. (a) Φ-rotor. (b) H-rotor. (c) V-rotor

1.2.4. Strut-Blade Connecting Fairing

Another parameter of the strut that should be considered is the geometry at the connection. When a blade is connected to a strut, a horseshoe vortex is generated at the "T" shape joint, resulting in greater wake extension[58]. This is one of the reasons for the degradation of the blade aerodynamic performance caused by the strut.

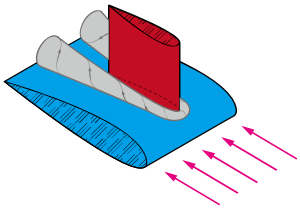

Fig. 5. The horseshoe vortex at the blade-strut connecting joint[24].

This performance loss could be reduced by using a fairing, which is a streamlined geometry that smoothly merges the blade and the strut at the connecting joint [24]. Hoerner [59] suggested using fairings with 4%~8% airfoil chord length circular radius as transition joints in aircraft design. The SANDIA labs added manual fairings to the blade joints of their 34 m VAWT, resulting in a small increase in performance in both low and high winds [11]. But their report did not provide details on the design of the fairing. Denis et al. [60] developed a 600 kW onshore VAWT with fairings, but also no details were provided. Thierry et al. [51] analyzed the effect of a circular transition between the end span strut and the blade, which was also considered as a fairing. They found that a radius of 0.5c works most effectively and could significantly decrease the kinetic energy of the vortex wake, which thus reduces the induced drag. Unfortunately, the effect of fairings on the performance of VAWT blades has not been sufficiently studied so far, especially the issue of matching different strut sizes to the fairing needs further investigation.

1.3. Present Work

1.3.1. Motivations and Objective

The above overview shows that the strut is an essential part of the VAWT, but it significantly affects the aerodynamic efficiency. Although some studies have been carried out, several issues still deserve future investigation.

To this end, the VAWT struts are investigated in this paper. The most aerodynamically efficient straight-bladed VAWT[6] is the subject of this paper. To balance the aerodynamic and structural performance, struts installed near the quarter span are used. Based on this, the strut parameters are numerically investigated to minimize their influence on the VAWT aerodynamic performance. The study focuses on the following issues:

- It is known that using streamlined profile reduces the strut drag. The drag characteristics of a strut profile is highly dependent on its chord length and relative thickness. However, discussions on these two parameters have not been conducted yet, and studies regarding their influence on the aerodynamic performance are still lacking in research. In addition, there is a periodic inversion of the pressure and suction sides of the VAWT blade. The influence of the struts on the different sides needs to be studied.
- At present, most of the strut use the same airfoil cross-sections as the VAWT blade, or a symmetrical NACA airfoil. However, it is still uncertain how to choose the strut profile size when the strut satisfies the structural strength. Are there other more suitable strut cross-sectional profiles?

- The effects of the strut connecting positions require confirmation. In particular, the influence of different chordwise positions has not been discussed when the strut chord length is smaller than the blade chord length.
- Inclined struts are frequently used in many large-scale VAWTs in recent years, but few analyses of have been published regarding their effects on the aerodynamic performance.
- How the connecting fairing between the strut and the blade affects the VAWT needs further study, especially the matching with different strut chord lengths.

In response to the above issues, this paper investigates VAWT struts, focusing on their influence on the aerodynamic performance. Using the parametric technology, nearly thirty different strut profiles including a novel low drag olivary shape were created by CAD method, and about eighty VAWT cases were calculated by 3D CFD simulation. The effects of chord length, thickness and area of struts were analyzed. Then the influences of the strut connecting configurations on VAWT aerodynamic performance were analyzed. This paper tried to provide some suggestions for the future VAWT strut design.

1.3.2. Organization of Present Study

The rest of this paper is organized as follows. Sections 2.1-2.2 present the geometrical and operational parameters of the baseline VAWT and the basic aerodynamic characteristics. Section 2.3 describes different strut parameters investigated in this paper, including the strut profiles (2.3.1), the spanwise and chordwise positions (2.3.2), the connecting angle (2.3.3) and the fairings (2.3.4). The models and settings required for the CFD approach, and the validations about mesh number, time step, revolution, turbulence model, and comparison of experimental data are presented in Sections 2.4-2.5.

The results are discussed in Section 3 in terms of the effect on both the aerodynamic performance and the fluid field characteristic. Section 3.1 analyzes the influence of the existence of the strut. The discussion in Sections 3.2-3.5 correspond to the different strut configurations in Section 2.3. The relatively optimal strut parameters are summarized in Section3.6. Finally, Sections 4-5 provide the conclusions and limitations of this paper, and further work that can be considered in the future.

2. Physical and Numerical Models

2.1. The Baseline VAWT Model

In this paper, a two-straight-bladed VAWT model of Li et al. [61, 62] is used, which provides elaborate experimental data to facilitate validation. Fig. 6 shows the VAWT model and the wind tunnel experimental facility [62]. The specifications of this VAWT are illustrated in Table 1.

Li et al. [40] did not provide the detailed parameters of the strut. Based on their image data[40], a thin and round-headed strut displayed in Fig. 6-(a) is created as a baseline wind turbine model. The strut has a chord length of $0.5c_B$ and a thickness of $0.01H$. A semicircular transition is used at both ends. The blade AC ($0.25c_B$) is located on the rotation radius. The center of the strut is connected to the $0.5c_B$ position of the blade. The influence of this chordwise connecting position will be discussed in subsequent sections. The tower diameter is the same as the blade chord length. The tower height is slightly higher than the strut position.

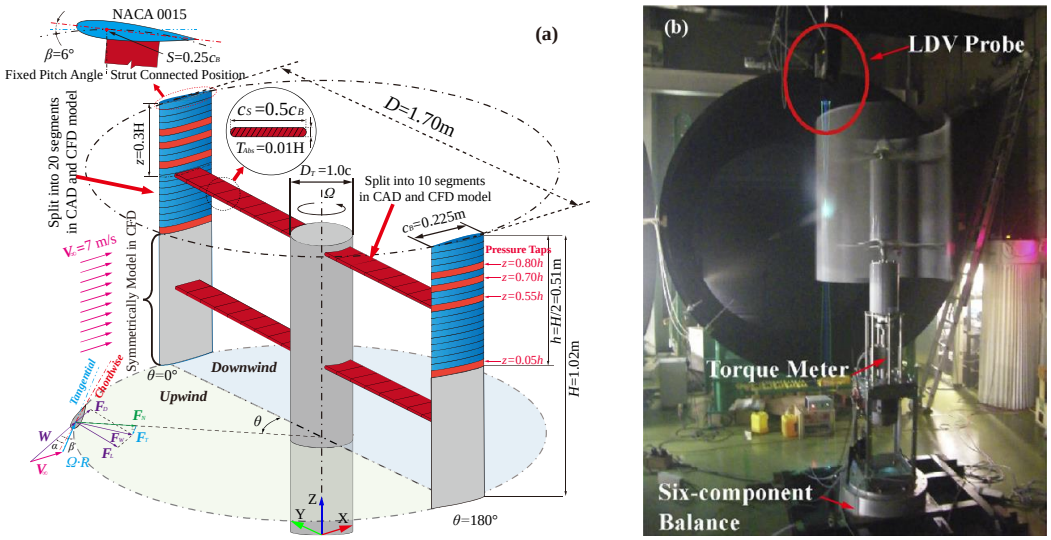

Fig. 6. The VAWT model and the tunnel experiment facility. The VAWT is simulated symmetrically. So the gray part of the blade are not meshed in the CFD model. (a) VAWT model with key specifications. Detailed parameters are seen in **Table 1**. (b) Experimental facilities from Ref [61, 62].

To facilitate comparison with the experiment, the baseline struts are fixed at 0.3H from the blade tip. Note that only half of the blade height is modeled, i.e., h=H/2=0.51m, while the other half is mapped in the CFD model using the symmetry plane boundary condition. This helps to speed up the simulation. Although the symmetric model results in a slight discrepancy at the bottom part of the tower, Aihara et al.[23] have shown that influence of the tower is relatively insignificant in the presence of struts.

The experimental blade were added with pressure measuring taps at four different heights of z=0h, 0.55h, 0.7h and 0.8h[39], as shown in Fig. 6-(a). In the numerical model of this paper, the blade and strut surfaces are split into 20 and 10 segments respectively, to monitor the forces varying along the span direction. This is also convenient to extract the data for four heights to compare experimental and simulation results.

Table 1 Geometrical and operational parameters of the VAWT.

Parameter	Value
Airfoil	NACA 0015
Blade Chord c_B	0.225 m
Strut position S	0.25c
Fixed pitch angle β	6°
Rotation diameter D	1.7 m
Blade Height H	1.02 m
Number of blades N	2
Solidity σ=Nc/D	0.265
Tower diameter D_T	c
Strut chord c_S	0.5c
Strut absolute thickness T_{Abs}	0.01H
Reynolds number Re	~2.30×10^5
Incoming velocity V_∞	7 m/s
Rotational speed Ω	15.23-20.75 rad/s
Tip Speed Ratio (TSR) λ	1.85-2.52

2.2. Aerodynamic Characteristics of Straight-Bladed VAWT

The aerodynamic characteristics of the straight-bladed VAWT cross-section is presented in Fig. 6-(a). We define θ as the azimuth angle, so 0°＜θ＜180° is called the upwind region and 180°＜θ＜360° is called the downwind region. V_∞ is the incoming wind speed, and Ω is defined as the rotational angular speed of the rotor. R is the rotor radius. The relationship between the tangential velocity ($\Omega \cdot R$) and incoming speed (V_∞) can be expressed by the tip speed ratio (TSR) λ:

$$\lambda = \frac{\Omega \cdot R}{V_\infty} \tag{1}$$

The normal force F_N and the tangential force F_T of the VAWT blade are calculated as following:

$$\begin{cases} F_T = F_L \sin(\alpha+\beta) - F_D \cos(\alpha+\beta) & (2) \\ F_N = F_L \cos(\alpha+\beta) + F_D \sin(\alpha+\beta) & (3) \end{cases}$$

where F_L and F_D are the lift and drag forces generated by the synthetic velocity of the incoming speed and tangential velocity, α and β are the angle of attack and the fixed pitch angle respectively.

The tangential force generates a torque Q, which is the power source of the VAWT. A VAWT with N blades can produce the power output P:

$$P = \Omega Q \quad (4)$$

$$Q = NF_{Ta}R \quad (5)$$

$$F_{Ta} = \frac{1}{2\pi}\int_0^{2\pi} F_T(\theta)d\theta \quad (6)$$

where F_{Ta} is the averaged tangential force of a single blade over one revolution.

Typically, we use the torque coefficient C_Q (Eq.(9)) and the power coefficient C_P (Eq.(10)) to evaluate the aerodynamic efficiency of VAWTs, which provides a convenient metric for different VAWTs [63].

$$C_Q = \frac{Q}{1/2\rho DHRV_\infty^2} \quad (7)$$

$$C_P = \frac{P}{1/2\rho DHV_\infty^3} \quad (8)$$

where ρ is the air density (assumed 1.18415 kg/m^3 in this paper), and other parameters as described in **Table 1**.

2.3. Strut Models with Different Configurations

2.3.1. Strut Profiles

The drag of a strut consists of profile drag and induced drag. The profile drag is caused by the frictional force and pressure difference generated by the strut profile. The induced drag is caused by the strut interfering with the flow on the blade surface. Apparently, the strut drags highly depends on its profile shape and size.

However, another key factor needs to be considered before investigating the strut drag characteristics, namely the structural properties of the strut. It should be strength enough to enable the strut to withstand the bending stresses generated by the blade weight and the axial stresses generated by the normal component of aerodynamic forces. For a horizontal strut, the internal stress σ_S can be approximated as[40]:

$$\sigma_S = F_N / A_S + M_y / I_x \quad (9)$$

where A_S is the cross-sectional area of the strut, M_y is the bending moment generated by the blade weight and the vertical component of the aerodynamic force, and I_x is the moment of inertia of the strut cross-section. Assuming the variation of strut profile does not affect F_N and M_y, the stresses on the strut are similar when the cross-sectional area is constant. Although the moment of inertia varies with the profile shape, it is still assumed to be the same here because the moment of inertia is strongly related to the cross-sectional area.

This equation suggests that the basic principle in analyzing the drag characteristics of different struts is to ensure that they have the same cross-sectional area, so that a fair comparison can be made. Therefore, a smaller chord length requires a larger relative thickness to ensure the same area, and vice versa. Based on this principle, the NACA XYZZ 4-digit series airfoils (ZZ is the thickness-chord ratio, TCR) which is most adopted in VAWT (both blades and struts) are used in this paper, to create various struts.

The blade cross-sectional area (A_B) is used as a reference. The strut cross-sectional areas (A_S) of different struts are classified as $0.5A_B$, $0.67A_B$, $0.75A_B$, $1.00A_B$ and $1.50A_B$. The strut chord lengths (c_S) are classified as $0.5c_B$, $0.75c_B$, $1.00c_B$, $1.25c_B$ and $1.50c_B$ based on the blade chord c_B. Once the strut area and chord length are defined, the relative thickness of the NACA 4-digit airfoil is determined. However, in this case, not all airfoil thicknesses are integers. Here a parametric description of the NACA airfoil profile is adopted in the form of a polynomial[64] and modeled in CAD software using a user-defined program. The airfoil polynomial is as follows:

$$\pm\frac{y}{c}=a_0\sqrt{\frac{x}{c}}+a_1\left(\frac{x}{c}\right)+a_2\left(\frac{x}{c}\right)^2+a_3\left(\frac{x}{c}\right)^3+a_4\left(\frac{x}{c}\right)^4 \tag{10}$$

where x, y are the airfoil horizontal and vertical coordinates, c is the chord length, a_0~a_4 are the coefficients. Taking NACA 0020 as an example, the coordinates are also subject to the following constraints:

(i) Maximum ordinate

$$\frac{x}{c}=0.3 \qquad \frac{y}{c}=0.1 \qquad \frac{dy}{dx}=0 \tag{11}$$

(ii) Ordinate at trailing edge：

$$\frac{x}{c}=1.0 \qquad \frac{y}{c}=0.002 \tag{12}$$

(iii) Trailing-edge angle：

$$\frac{x}{c}=1.0 \qquad \frac{dy}{dx}=0.234 \tag{13}$$

(iv) Nose shape：

$$\frac{x}{c}=0.1 \qquad \frac{y}{c}=0.078 \tag{14}$$

The coefficients a_0= 0.2969, a_1= -0.1260, a_2= -0.3516, a_3 = 0.2843 and a_4= -0.1015 are obtained by above equations. Airfoils with different TCRs are created by adjusting the value of y/c. Twenty-two NACA airfoils are shown in Table 2. For comparison purposes, the strut thickness is defined as a dimensionless parameter of the ratio of the absolute thickness to the blade height T_{abs}/H, where $T_{abs}=c_S\cdot$TCR.

Table 2 The cross sections of VAWT struts with different profiles, areas, chord lengths, and thicknesses analyzed in this paper. Taking the NACA airfoil in rows 1-6 as an example, the first row indicates the ratio of the strut chord (c_S) to the blade chord (c_B), while the first column indicates the strut cross-sectional area (A_S) to the blade cross-sectional area (A_B). Thus, the cross section of strut in the 2nd row and 2nd column has an area A_S=0.5A_B and a chord length c_S=0.5c_B. The absolute thickness (T_{abs}) of the strut is represented as a ratio relative to the blade height (H). Several profiles with pentagrams have the same absolute thickness and are used for comparison in later sections. The olivary struts in rows 8-11 are defined by the same rules, where $D_{S\text{-}LE}$ in the 5th column is the leading/trailing edge diameter. The last two columns of rows 8-11 are used for the strut of the baseline wind turbine.

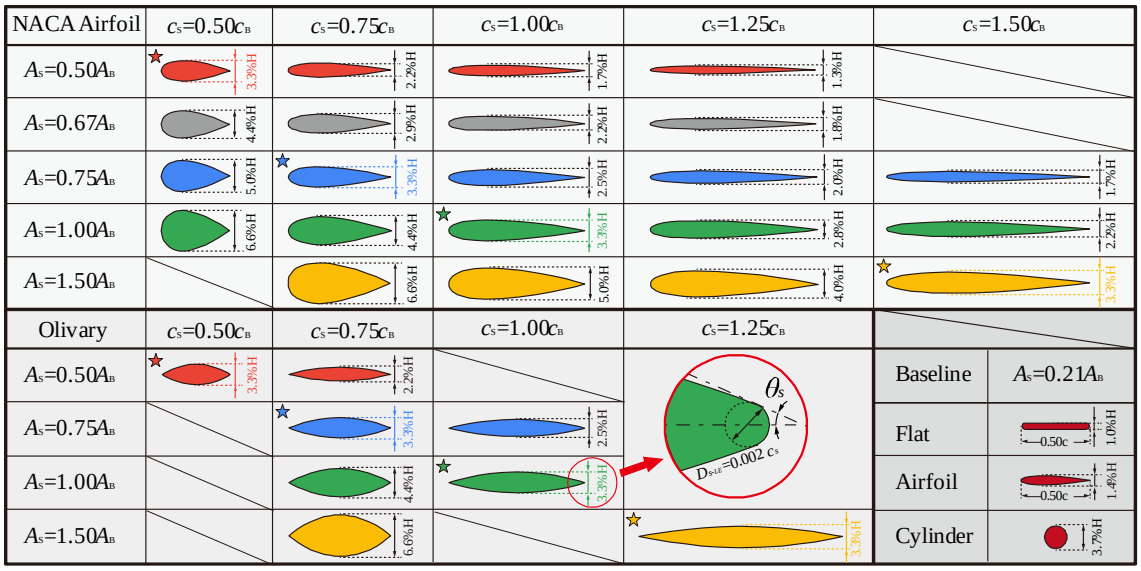

In addition to the NACA series airfoil, a symmetrical olivary-shaped profile (see the left-bottom part of Table 2.) is proposed specifically for the VAWT struts, which has lower drag characteristics and can be fabricated simply. Two reasons motivate the design of this olivary profile:

(i) Lift performance is not the primary function of a VAWT strut. Therefore, the NACA 4-digital series airfoil with a high maximum lift coefficient is not necessary and not suitable for a strut. Since the relatively large diameter of the NACA airfoil leading edge is not beneficial for drag reduction, the leading edge section is

modified to a similar size as the trailing edge.

(ii) The struts of a large-scale VAWT prefer to be manufactured as a hollow structure using composite materials similar to the HAWT blade. This composite structure is supported by the internal spars and shear webs, where the spars are usually located at the maximum thickness position (MTP). However, the maximum thickness of the NACA airfoil is at $0.3c_B$, resulting in a forward center of gravity and a large panel area in the trailing edge region, which is susceptible to buckling. Therefore, a centrosymmetric profile looks like an olive-shape core is proposed.

The maximum thickness of the olivary profile is the same as that of the NACA airfoil, following Equation (11). Both leading and trailing edges follow Equation (12), but with a circlar transition between upper and lower surface. To make a fair comparison, the values of the tangent angle θ_s for the olivary leading and trailing edges are varied to change the profile curve curvature, so that the olivary profile has the same area as the NACA airfoil when their TCRs are the same. Besides, the profiles in the right-bottom of Table 2 in dark red are the NACA airfoil and cylindrical struts with the same area as the baseline flat experimental VAWT model, which are also used to analyze the effects caused by the profile geometry.

The three-dimensional model of the struts with different chord lengths are illustrated in Fig. 7. When $c_s \leq 1.00c_B$, the ACs of the blade and the strut are overlapped. When $c_s > 1.00c_B$, the strut will extend a distance so that it wraps around both sides of the blade as seen in Fig. 7 (d), which is common in some small or experimental wind turbines[65].

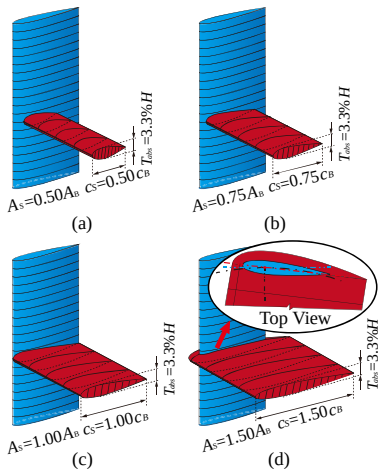

Fig. 7. Three-dimensional geometric model of struts with different chord lengths. The spanwise connecting position is the same as the baseline model. (a) $c_S=0.50c_B$; (b) $c_S=0.75c_B$; (c) $c_S=1.00c_B$; (d) $c_S=1.50c_B$.

It should be noted that those extremely thin struts (with small TCR) in Table 2 are feasible for small VAWTs because of their low aerodynamic forces and blade weight. Such thin struts have been used in many experimental turbines[65, 66]. However, as the size of VAWT increases, the blade weight and aerodynamic forces will increase by cubic and quadratic orders of magnitude of the size, respectively. Apparently, such thin struts are not practical for large-scale VAWTs because it is difficult to fabricate and provide support. Nevertheless, for this paper, designing these extremely thin strut profiles is still valuable, as this allows analyzing the effect of strut geometry on the blade aerodynamic performance.

Moreover, in practice, large VAWT struts prefer variable cross-sections like HAWT blades, i.e., thicker airfoils at the root to provide more strength, and progressively decreasing thickness along the spanwise direction to reduce drag. However, this would lead to too many parameters and increase the complexity of the analysis, so the constant cross-sectional area is used in this paper to facilitate comparison.

2.3.2. Strut Connecting Positions

(i) The Spanwise Position

As mentioned, this paper is aimed at the strut installed near the quarter span position. Mojtaba et al.[40] showed that the structural stresses in the blade are minimize when the strut are installed at 0.2H position from the blade tip. On the other hand, to facilitate comparison with the reference experimental model, the baseline VAWT struts are installed at the 0.3H position in this paper.

Therefore, the effects of these two spanwise positions are compared here, as shown in Fig. 8. Eight struts are modeled at the 0.2H position: the NACA airfoils and the olivary profiles (marked with pentagrams with absolute thickness of 3.3%H in Table 2). Other connecting parameters are identical to 0.3H cases if the profile is the same.

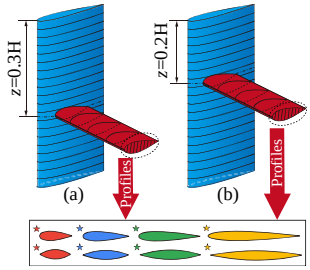

Fig. 8. Different spanwise connecting position of struts for various NACA and olivary profiles. All struts keep the same absolute thickness of 3.3%H but have different chords. (a) z=0.3H. (b) z=0.2H.

(ii)The Chordwise Positions

Previous studies on the connecting position have focused on the relative position of the blade AC to the rotor center. However, the effect of different chordwise connecting position in the 3D case is neglected when the strut chord length is smaller than the blade chord length.

Therefore, the different strut chordwise connecting positions are modeled as illustrated in Fig. 9. Three profiles of the baseline flat, NACA airfoil (two chord lengths of c_S=0.50c_B and c_S=0.75c_B, both A_S=0.5A_B) and the olivary (c_S=0.50c_B, A_S=0.5A_B) are analyzed so as to exclude the influence of profile shape. The ACs of all blades are located on the same radius. Here the d_{LE} and d_{MTP} are used to define the chordwise positions of struts. These two parameters are helpful to investigate the flow mechanism for the different profiles, which will be discussed in detail in later sections.

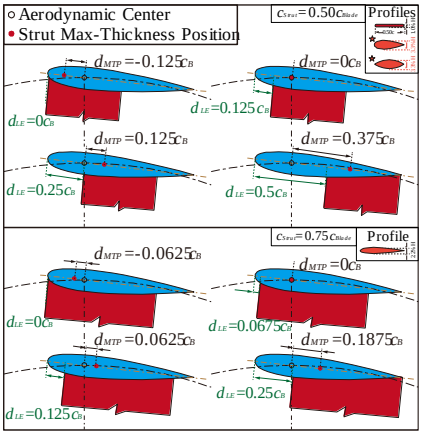

Fig. 9. Different chordwise connecting position of struts. The d_{LE} represents the distance between the blade leading edge and the strut leading edge. The d_{MTP} represents the distance between the strut MTP and the blade AC. For the situation of c_S=0.50c_B, three profiles as shown in right-top are used. For the situation of c_S=0.75c_B, only the NACA profile is used.

2.3.3. Strut Connecting Angle

The effect of strut angle on the aerodynamic performance of the VAWT is analyzed according to the inclined strut, as shown in Fig. 10. One principle of the inclined strut is to make the tower height in the middle of the blade. This allows the load on the strut to be balanced. This principle leads to the strut angle being decided when the rotor radius, the blade height and the spanwise connecting position are determined. In this paper, the inclined strut angle

is 15°. As in the case of the spanwise position investigation, a total of eight profiles of the VAWT model with inclined strut are designed.

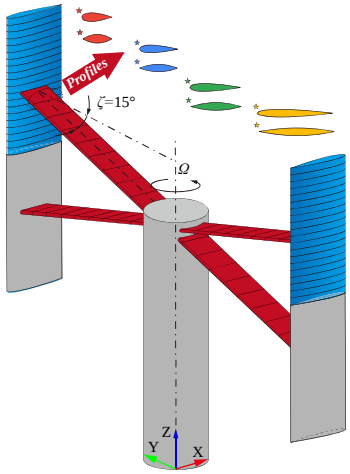

Fig. 10. The VAWT model with inclined struts. It is also simulated using symmetric boundary condition. Various NACA and olivary profiles are used. All struts keep the same absolute thickness of 3.3%H but have different chords.

2.3.4. Strut-Blade Connecting Fairings

To analyze the effect of fairing, a circular transition surface at the connecting conner between the strut and the blade is used. Hand et al. [24] suggested that the fillet radius r=0.06c_B. Here two radiuses, r=0.06c_B and r=0.12c_B are analyzed. The fairings for struts of different chord lengths are shown in Fig. 11. Among these the case of c_S=1.00c_B is special. Since the circular transition surface results in a bunt trailing edge with a large thickness, a distance must be extended to achieve a streamlined shape. This design is similar to the fairing in Ref. [60].

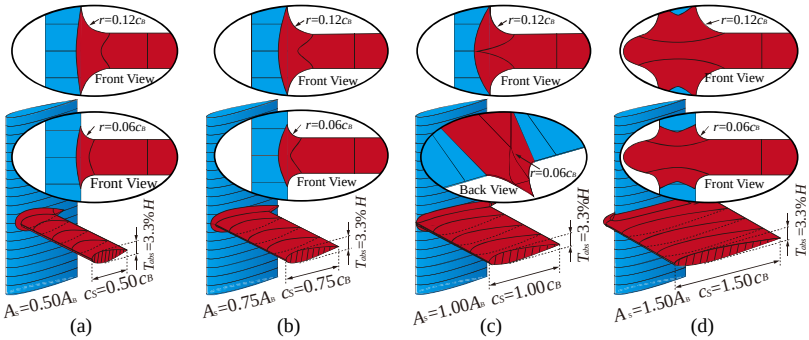

Fig. 11. The strut-blade connecting fairings for different strut chords and fairing radiuses. Both the NACA and olivary profiles are used, but here only show the former. All struts also use the profiles with pentagrams as described in **Table 2**. (a) c_S=0.50c_B; (b) c_S=0.75c_B; (c) c_S=1.00c_B; (d) c_S=1.50c_B.

2.4. CFD Model

2.4.1. Boundary Conditions and Mesh Topology

In this paper, CFD simulations are performed using Star-CCM+. Fig. 12 displays the computational domain and boundary conditions. In the top left figure, 5D or 8D represent distance of five or eight times the rotor diameter, which is far enough to minimize the boundary reflection effect [67]. The bottom surface uses the symmetry plane condition to map the half blade as mentioned above. The left, right and top surfaces use the slip wall condition to avoid the influence of wall boundary as Zhang et al. [13] did. The velocity inlet condition of 7 m/s inflow speed and the pressure outlet condition for standard atmospheric pressure are employed on the front and back surfaces respectively. The inner interface condition is used to connect the rotating region to the stationary region, while the rotating region use a sliding mesh method to simulate rotor rotation. Other sub-figures show the mesh topology. There are 24 layers of prism meshes around the blade surface with the first layer having a height of 0.0015 mm, which makes the y+ ~1 to deal with the sub-layer of wall boundary layer. Three levels of local mesh refinements

are used to better capture the flow characteristics in the wake.

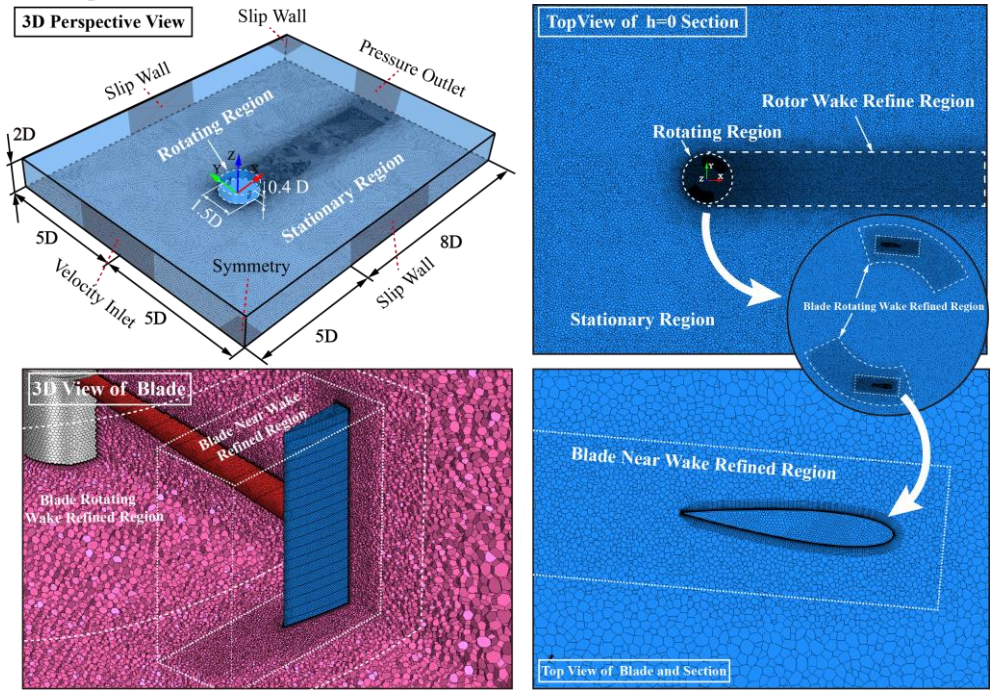

Fig. 12. An illustration of the computational domain, the boundary conditions and the mesh topology. The white dashed lines in sub-figure show the local mesh refinement. Three levels of refinement in total, which are the blade near wake refined region, the blade rotating wake refined region and the rotor wake refined region.

2.4.2. Solver Settings

Considering small velocity and the absence of heat diffusion in VAWT simulations, the implicit segregated flow model of an incompressible constant density gas is used to solve the flow equations without energy. The pressure-velocity coupling is combined with a SIMPLE-type algorithm and the second-order upwind schemes is applied for velocity, pressure, and turbulence. The second-order upwind scheme is set to the convection term. In the unsteady simulation, a second-order central difference scheme is used for temporal time discretization. All simulations were adopted 10 inner-iterations at each time step and were carried out on in-house parallel computing server with 10 nodes. Node 1st is used for system management and the remaining nine nodes can be used for CFD calculations. Each node is equipped with two Intel (R) Xeon (R) Silver 4116 CPU @ 2.10 GHz processors with eighteen cores each. Each node has 128GB of memory. For a single VAWT model, a complete converged CFD simulation with a single node of 36 cores takes approximately 80 hours. If three nodes of 108 cores are used, the computing time for a single case can be reduced to 24 hours.

2.5. Validation of Simulations

Verifying numerical models to improve their reliability is essential for simulation studies. Our previous study[12] provided comprehensive numerical simulation validations, including grid convergence, time step, rotor revolution, turbulence model and comparison with experimental values. The numerical model for this paper uses the same strategy as the previous ones. Therefore, a brief description of the numerical model setup is presented here. The complete validation details can be found in Ref. [12].

2.5.1. Grid Convergence Study

Methods for examining the grid convergence of CFD simulations are presented in the book by Roache [68], which is based on the Richardson's extrapolation method. It should perform simulations on several successively finer grids. Zadeh et al. [69] provided a detailed process for VAWT meshes. Table 3 shows the grid convergence study of the VAWT without struts at two TSRs in the validation study[12].

The *ARC* of 1.0048 for λ=1.85 and 1.0329 for λ=2.29, are close to 1, indicating that the results are in the range

of asymptotic convergence. The maximum error $GCI_{i+1,i}^{fine}$ are 0.014% for λ=1.85 and 0.497% for λ=2.29, both simulations are below than 3%. This indicates that further refinement of the mesh size does not markedly improve the accuracy of the calculations, and the medium mesh is fine enough. Therefore, all VAWTs with struts use the medium mesh strategy in this paper.

Table 3. Discretization error for λ=1.85 and λ=2.29. The critical variable f_i is used to verify the influence of mesh refinement based on the simulation result. The power coefficient (C_P) of VAWT is used here. All parameters on the left are coefficients required for GCI calculation.

Parameters	Value	
	λ=1.85	λ=2.29
Fine Mesh Number (N1)	5,319,717	
Medium Mesh Number (N2)	3,589,852	
Coarse Mesh Number (N3)	2,916,044	
r_{21}	1.5	1.5
r_{32}	1.5	1.5
f_1	0.1416	0.3085
f_2	0.1410	0.2987
f_3	0.1110	0.2102
ε_{32}	-0.0300	-0.0885
ε_{21}	-0.0007	-0.0098
p	9.3636	5.4200
R	0.0224	0.1111
e_a^{21}	0.475%	3.185%
e_a^{32}	21.252%	29.619%
GCI_{21}^{Fine}	0.014%	0.497%
GCI_{32}^{Medium}	0.610%	4.626%
ARC	1.0048	1.0329

2.5.2. Time Step and Revolution Verification

According to the study of Rezaeiha et al. [70], the azimuthal increments corresponding to the time step and rotor revolutions will affect the accuracy of the VAWT simulations.

For wind turbine simulations, the azimuthal increment associated with the rotating speed Ω is used to verify the time step. Four different azimuthal increments include Ωdt=4°, 2°, 1° and 0.5° were tested[12]. Considering the computational efficiency and simulation accuracy, the azimuthal increment Ωdt=1° was used finally.

The revolution verification of wind turbine simulations is essential because the wake from the upwind moves downstream and thereby affecting the aerodynamic performance of the VAWT blades. Therefore, the number of rotor revolutions should be tested to ensure the simulation obtains a statistically steady state. The revolution was verified by monitoring the variation of C_P. Most cases get a statistically steady state after the 6th revolutions[12], which is the same as Ref. [13]. But for some cases with fluctuations, a few additional revolutions were calculated.

2.5.3. Turbulence Model Verification

The turbulence model has a remarkable influence on CFD simulations. It is recognized that the *k-ω* shear stress transport (SST) model in the unsteady Reynolds-averaged Navier-Stokes (URANS) equations is suitable for VAWT simulations [71, 72]. However, it is mostly studied in 2D simulations. Rezaeiha et al.[73] showed that the accuracy of URANS is not sufficient for 3D VAWT simulations, while the hybrid RANS/LES model can better capture the dynamic stall and the vortex characteristics in the wake. Therefore, the Improved Detached Eddy Simulation (IDDES) [74] model based on the *k-ω* SST model and RANS turbulence model were verified. Previous turbulence model verification showed that IDDES does have better agreement with the experimental data[12, 75]. Therefore, the IDDES model is adopted in this paper.

2.5.4. Validation Using Experimental Data

Finally, the simulation results are verified with experimental data. Fig. 13 shows the pressure coefficients C_{Pre} at the blade center position z=0h for different azimuthal angles when λ=2.29. The inflow velocity V_∞=7 *m/s* was

used to calculate the pressure coefficient. The present CFD result uses the medium mesh with 1°azimuthal increment, IDDES model and the sampled data of the 6th revolution. As illustrated in Fig. 13, the pressure coefficients show a good arrangement with the experiment at most azimuthal angles.

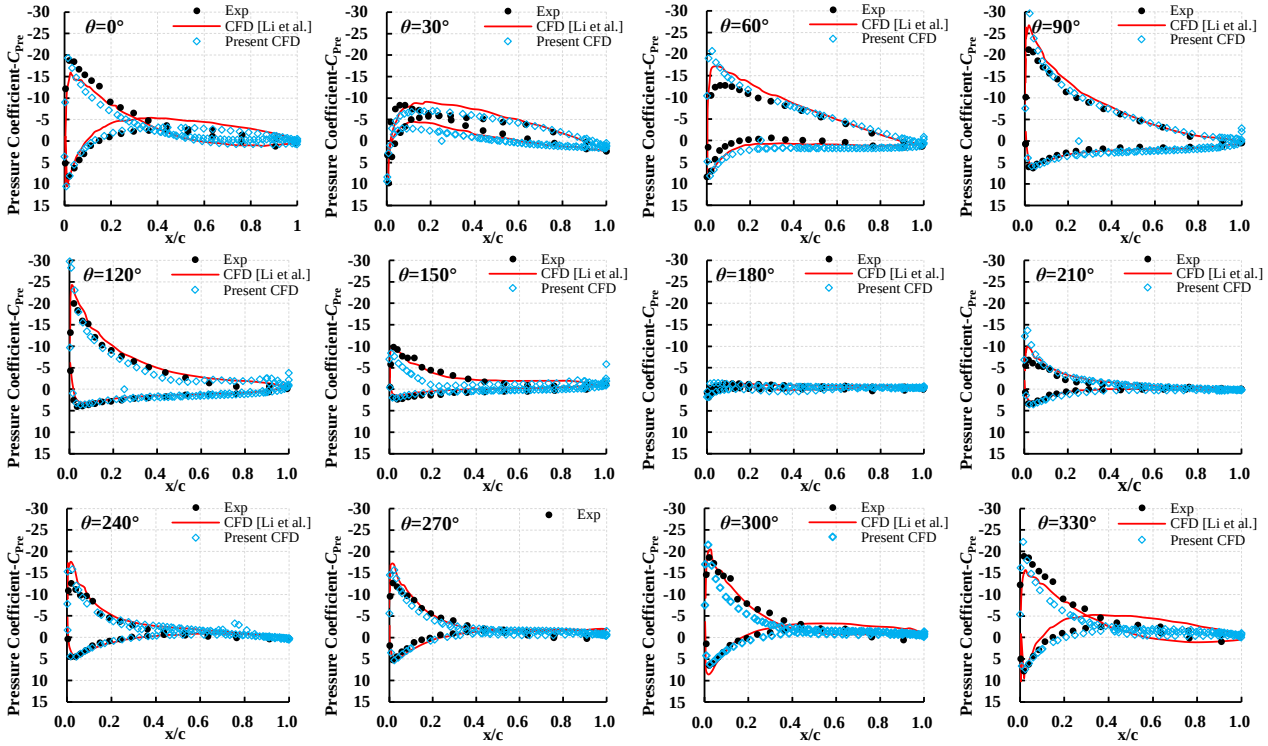

Fig. 13. Pressure coefficient distribution on the blade center position z=0h, λ=2.29. The black dot and red line are the experimental data and CFD simulation result of Li et al. [61]. The blue lattice proves the accuracy between present CFD simulation and the experimental value.

The torque coefficients of the experiment and the baseline model with flat struts at different heights are shown in Fig. 14. At z=0.05h, the baseline model is in good agreement with the experiment data. As the height close to the blade tip, the simulated C_Q are slightly higher. This variation may be caused by the different positions of the strut connection. However, the phenomenon that C_Q significantly decrease near the strut is the same in both the experiment and the simulation.

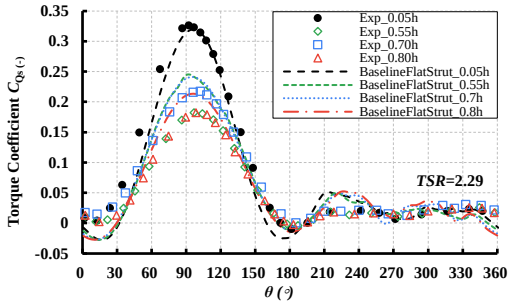

Fig. 14. Torque coefficients (C_Q) of the experiment and the baseline model with flat struts at different blade pressure tap heights.

The above validation studies prove that the CFD simulation in this paper has a good accuracy compared with the experimental data, which guarantees the effectiveness of the subsequent simulations.

3. Results and Discussion

3.1. The Strut Effects

The variation of the aerodynamic performances of VAWTs with and without struts are analyzed firstly. Three baseline struts in the right-down of Table 2 are compared here. Their cross-sectional profiles are flat bar, NACA

airfoil and cylinder respectively.

(i) Aerodynamic Performance

The power coefficients of the baseline wind turbine at different TSRs are shown in Fig. 15. Two important results can be obtained:

- The presence of struts substantially reduces the VAWT efficiency. In sub-figure (a), it is observed that the C_P is overestimated when the strut (green curve) is neglected in the numerical simulation, which is one of the reasons why many 2D simulations are much higher than the experimental values. When the simulation considers struts, the total C_P of the whole baseline VAWT (red curve, the total torque including struts and tower) and the blade C_P (blue curve, calculating torque only from blades) show good agreement with the trendy of the experimental value (black triangles, integrating the value from the blade pressure taps). This also proves the accuracy of the numerical simulations in this paper. Besides, the experiment also tested the C_P of the whole VAWT (yellow diamond) by means of a six-component balance. However, these values are even lower since there is mechanical damping between experimental parts, which leads to a further power loss. This loss is difficult to be calculated in CFD simulations.
- For these three struts with the same cross-sectional area, it indicates that the strut cross-section profile shapes have a significant influence on the aerodynamic efficiency, as shown in sub-figure (b). The $\Delta C_{P\text{-Profile}}$ and $\Delta C_{P\text{-Induced}}$ values are close for the non-streamlined struts (the flat and cylinder), while both the profile and induced drags of the cylinder strut are significant, resulting in a negative total efficiency. For the streamlined airfoil strut with similar chord and thickness to the flat strut, both direct and induced drag can be reduced, especially for the former.

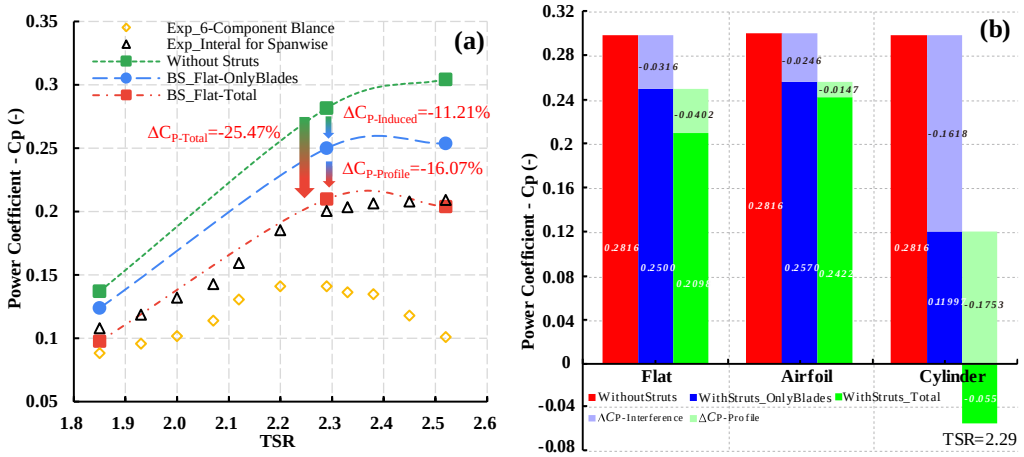

Fig. 15. Power coefficients of the baseline VAWTs. (a) C_P of the flat strut VAWT at different TSR. The black triangles are the integral of the spanwise pressure taps in experiment. The yellow diamonds are experimental data obtained from 6-component balance. Other colors are simulated results. (b) C_P of the simulated baseline VAWTs with different strut profiles at TSR=2.29. $\Delta C_{P\text{-Induced}}$ indicates the efficiency reduction caused by the variation of the blade torque in the presence of the strut, which is the induced drag. $\Delta C_{P\text{-Profile}}$ indicates the efficiency reduction due to the drag of the strut itself, which is the direct drag.

To investigate the influence of strut at different azimuth angles, the C_Q of a single VAWT blade without and with struts is displayed. Fig. 16 shows the torque coefficients of the whole blade, while Fig. 17 shows the torque coefficients for each segment at different blade heights (20 segments in total). It can be observed that:

- The distributions of the two drags are completely different at various azimuth angles, as shown in the light red and light blue areas in Fig. 16, respectively. The induced drag is concentrated at $60^\circ<\theta<180^\circ$ (when the strut is on the suction side of the VAWT blade), while the profile drag is more significant at $0^\circ<\theta<30^\circ$ and $270^\circ<\theta<360^\circ$ (when the relative wind speed of the strut is higher).
- The strut affects a wide range in the spanwise direction of the blade. Comparing Fig. 17 (a) and (b), it is observed that the blade C_Q has a significant reduction at the strut connecting position. Fig. 17 (c) shows the variation of C_Q for VAWT blade with and without struts. This variation represents the induced drag caused

by the flat strut. It is observed that in the upwind region, the influence of the strut spreads from the blade middle (0.0h) to the tip (1.0h), despite its installation at 0.45h. In the downwind region, the influence of the strut is relatively small, and there is even a slight increase in C_Q near the blade tip part at 240°<θ<300°. This increase is most likely due to the local velocity variation caused by the blade tip vortex.

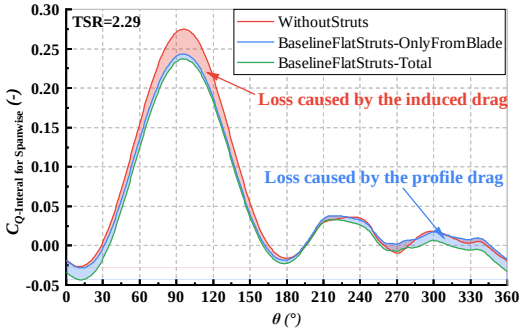

Fig. 16. Torque coefficients of the VAWT single blade without and with strut at TSR=2.29. The light red and light blue areas indicate the torque losses caused by the induced drag and the profile drag, respectively

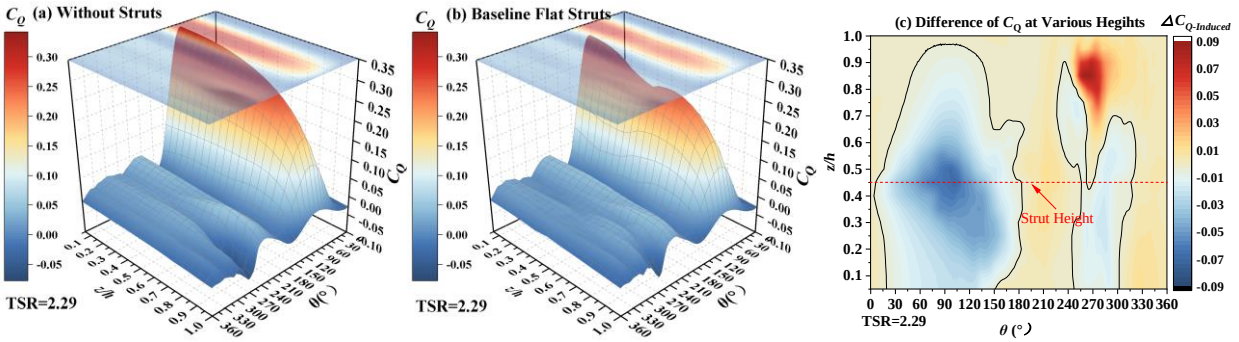

Fig. 17. Torque coefficients of single blade varying along the spanwise direction at TSR=2.29. **(a)** the blade without struts; **(b)** the blade with flat struts, but the C_Q values are only from blade; **(c)** Difference of torque coefficients ($\Delta C_{Q\text{-Induced}}$) between the blades without and with flat struts. The blue area shows the spatial location where the blade torque coefficient decreases, and the boundaries of this area are identified using contours.

(ii) Fluid Field Characteristics

The effects of the struts on the fluid field characteristics and the blade surface streamlines are displayed in Fig. 18. The surface streamlines can be used to determine whether the fluid attaches to the blade surface to generate aerodynamic forces. The cylinder strut is also shown here. From the perspective of the pressure and suction surfaces of the VAWT blade:

- For the pressure side, the influence of the strut is not significant as seen by the blade surface limited streamlines in Fig. 18 (a), (c) and (e). In the downwind region at θ=270°, the flat and cylinder struts only interfere with the blade pressure surface flow within their thickness range. In the upwind region at θ=90°, both struts barely affect the blade surface flow.
- For the suction side, the impact of the struts is extremely pronounced. In the upwind region at θ=90°, the flow separation occurs at the strut position, resulting in a reduction of the blade aerodynamic force. This separation is much larger than the thickness range of the strut, which is clearly related to the shedding vortex scale induced by the strut cross section shape. In the downwind region at θ = 270°, the strut still affects the blade suction side, although it is located on the opposite (pressure) side at this point. Importantly, it is observed in the lower left corner of Fig. 18 (b) and (d) that the streamlines near the flat strut blade tip are instead better attached than the blade without strut, as confirmed by the C_Q curves in Fig. 16. For the cylinder strut, the flow on the suction side is almost completely separated at θ = 270°. Combined with the vorticity field, the presence of the struts significantly aggravates the vortex scale and intensity of the VAWT wake.

As seen above, for the VAWT with struts, the reduction in aerodynamic performance is primarily caused by

the struts interfering with the blade suction surface in the upwind region, while in the downwind region it is caused by the changes in the wake induced by the struts.

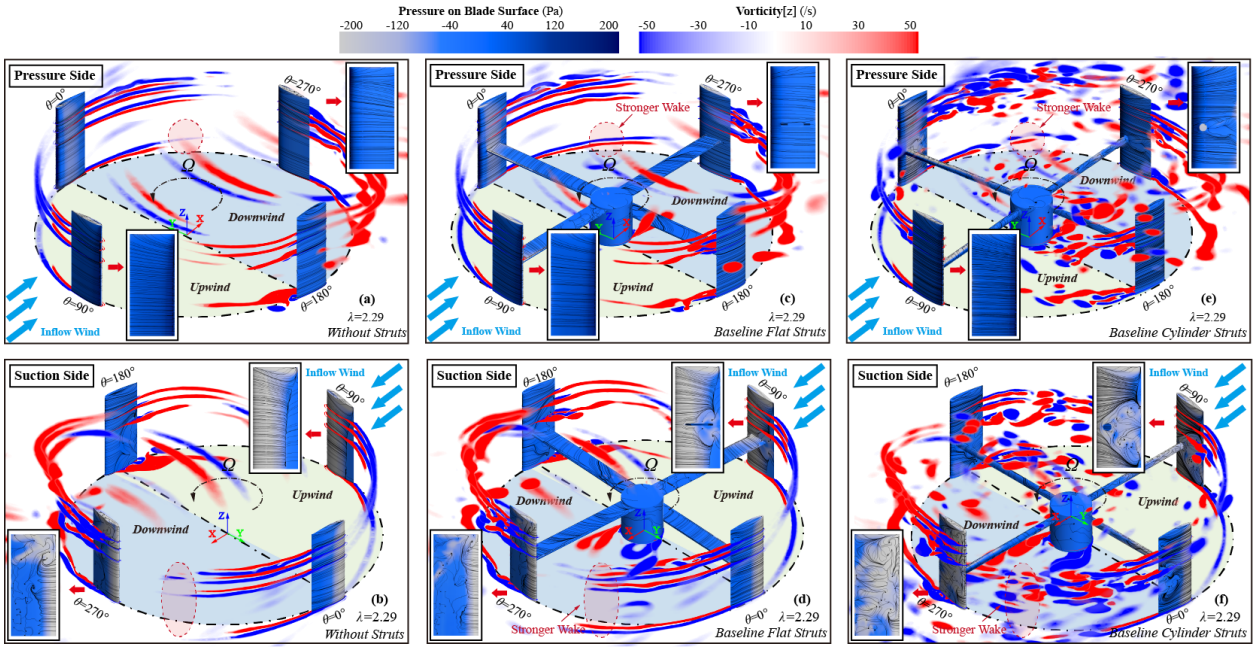

Fig. 18. Flow characteristics of the VAWTs without struts, with flat struts and with cylinder flats at TSR=2.29. The surfaces of blades and struts are colored in static pressure and covered with the limited streamlines. The z-vorticity at z=0h, z=0.55h, z=0.7h and z=0.8h in the fluid field are also displayed to show the wake.

3.2. Influences of Strut Profiles

The influence of the strut profiles is discussed here, focusing on the variations of chord, thickness, and cross-sectional area. In addition, the performance of the specialized strut profile proposed in this paper is analyzed.

3.2.1. Effects of Chords, Thicknesses and Areas

(i) Aerodynamic Performance

Fig.19 illustrates the C_P of VAWTs for NACA airfoil struts with different chords, thicknesses and areas. Several results are observed:

- The VAWT efficiency decreases obviously with the increase of the strut cross-sectional area. For the struts with same area, their profile drags increase as the relative thickness increases (with a corresponding decrease in chord), which essentially follows an exponential power low, as shown in Fig. 19 (b). This is determined by the drag characteristics of the NACA airfoil itself[76]. However, an interesting phenomenon is that, when $A_{Strut}/A_{Blade}\leq 1.0$, the total C_P suddenly decreases at $c_{Strut}/c_{Blade}=1.0$, as shown by the red circle in Fig. 19 (a). In addition, this phenomenon is also observed for struts with the same absolute thickness ($T_{Strut}/H_{Blade}=3.3\%$) but different chord lengths
- The drag magnitude of the VAWT strut is approximately linearly related to the strut absolute thickness. As illustrated in Fig. 19 (c), all C_P values representing the NACA airfoil struts are located within the narrow red region. This linear relationship is not obvious if the horizontal coordinates are replaced by relative thicknesses, as seen in Fig. 19 (d).

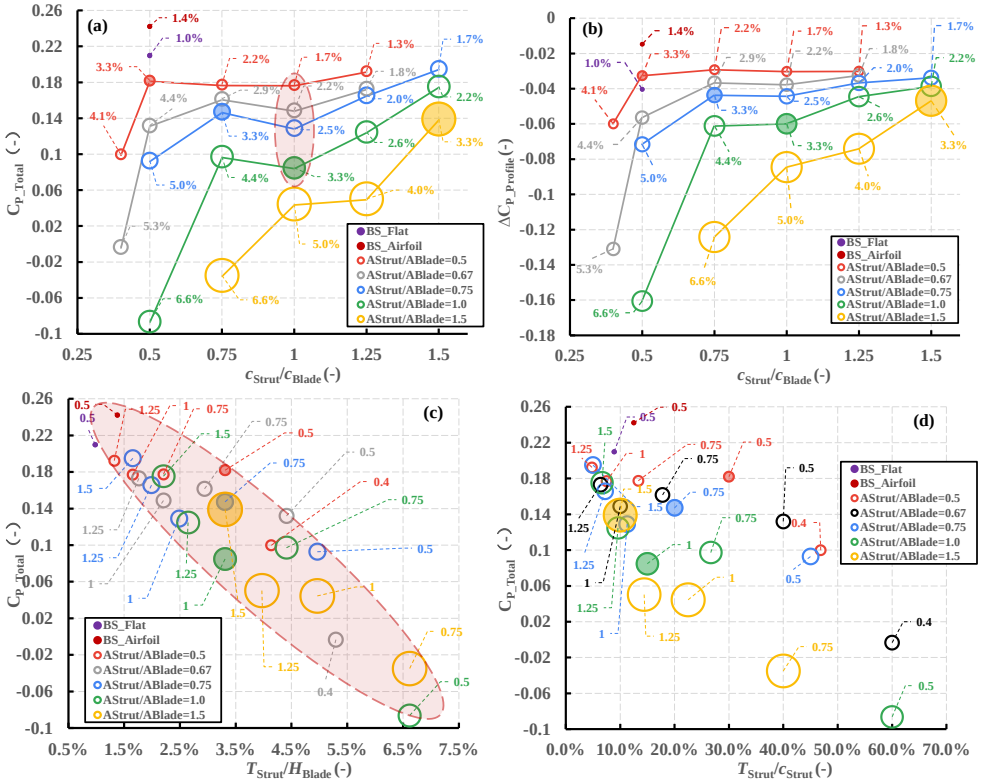

Fig. 19. C_P of VAWTs with different chord lengths and thicknesses NACA airfoils struts. The bubble diameter represents A_{Strut}/A_{Blade}, (a) The total C_P varies with c_{Strut}/c_{Blade}, the label value represents the absolute thickness ratio T_{Strut}/H_{Blade}. (b) The power losses caused by the strut profiles drags. (c) The total C_P varies with T_{Strut}/H_{Blade}, the label value represents the relative thickness c_{Strut}/c_{Blade}. (d) The total C_P varies with the relative thickness T_{Strut}/c_{Strut}.

The blade C_Q curves for the struts with same areas A_{Strut}=0.75A_{Blade} but different chords are shown in Fig. 20 (a). When c_S=1.00c_B, the blade torque in the upwind region is significantly reduced, even lower than the case of c_S=0.50c_B with the maximum relative thickness. Fig. 20 (b) shows the difference in C_Q at various heights for c_S=1.00c_B and c_S=0.75c_B, and it indicates that the torque reduction in the former occurs mostly on the blade surface above the strut when 60°<θ<180°.

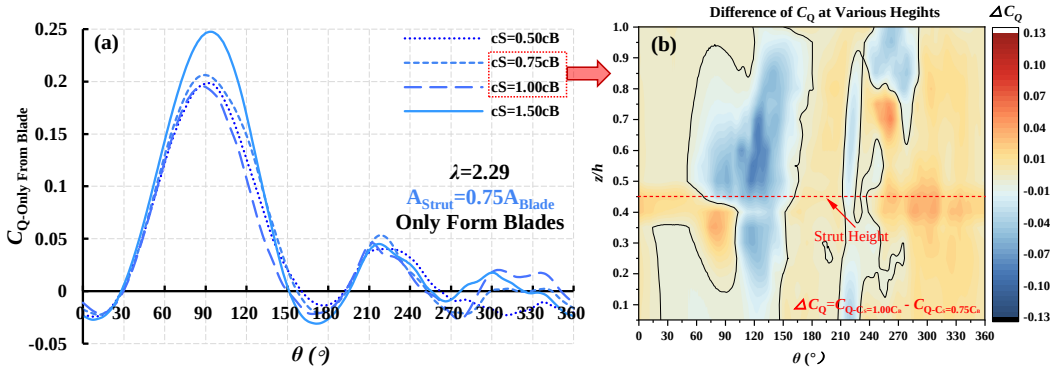

Fig. 20. Torque coefficients (C_Q) when A_{Strut}=0.75A_{Blade}. (a) C_Q of the single blades for different strut chords. (b) ΔC_Q is the difference between the blade struts c_S=0.75c_B and c_S=1.00c_B along the blade spanwise direction.

(ii) Fluid Field Characteristics

To investigate the effect of strut size on the flow characteristics, the surface limited streamlines and Q-criterion iso-surfaces for blades with different chords (and thickness) are extracted at θ = 120°, as shown in Fig. 21. This azimuth angle is selected because the C_Q curves indicate a large difference in the performance of each blade at this upwind position. Several results are found:

- The strut chord is an important factor affecting the flow characteristics of the blade surface. By vertically comparing any two cases, such as (a) with (e), (b) with (f), etc., it is observed that the limited streamlines and the shedding vortices around the struts are similar as long as the struts have the same chord, regardless

of whether the thickness (or cross-sectional area) is the same.

- When the strut chord is equal to the blade chord, i.e., c_S=1.00c_B, the flow separation on the blade surface is remarkable. As seen in Fig. 21 (c) and (g), the vortex scales and their influence range on the blade surface along the spanwise direction are the largest among these cases. Compared to the streamlines, the separation occurs earlier in the region of blade leading edge above the strut when c_S=1.00c_B, as illustrated in the red dashed lines.
- When the strut chord is longer than the blade chord, the vortex formed at the connection is significantly reduced. Comparing Fig. 21 (e)~(h), the increase in chord increases the cross-sectional area for the same absolute thickness, but the streamlines at c_S=1.5c_B is similar to that at c_S=0.50c_B, with the former having less separation at the blade leading edge. This phenomenon implies that the strut chord length exceeding the blade chord length may also be a good choice.

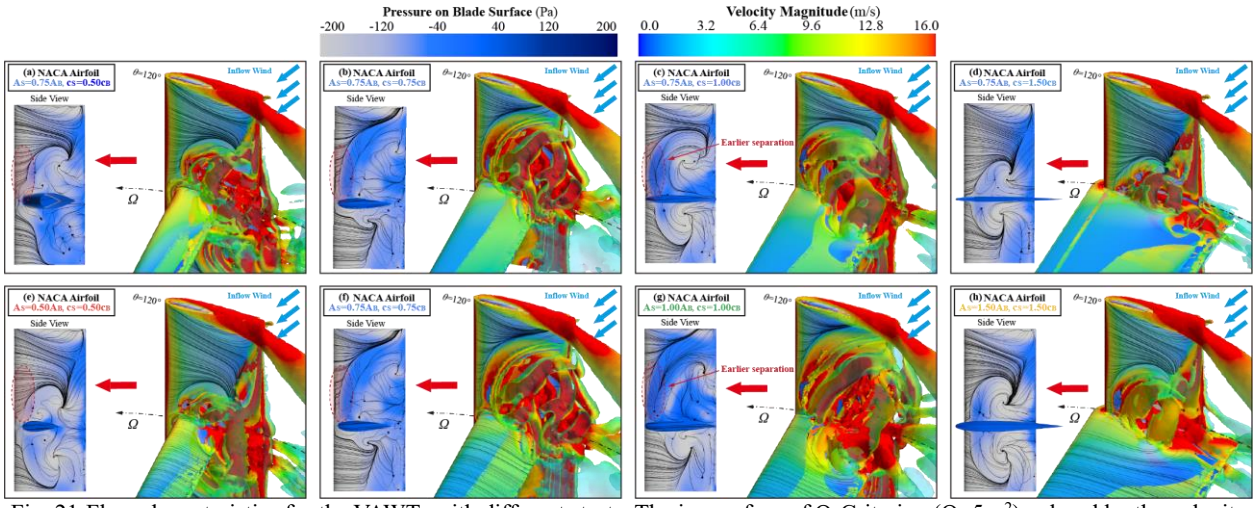

Fig. 21 Flow characteristics for the VAWTs with different struts. The iso-surface of Q-Criterion (Q=5 s^{-2}) colored by the velocity magnitude are used to display the vortex around the blade. (a)~(d) Struts have same areas of A_{Strut}=0.75A_{Blade}. (e)~(h) Struts have same absolutely thickness of T_{Strut}=3.3% H_{Blade}.

3.2.2. The Olivary Profiles

(i) Aerodynamic Performance

Based on the characteristics of the VAWT strut, an olivary-shaped specialized profile is proposed in this paper. Several olivary struts with different areas and chords in Table 2 are calculated. The power coefficients of these VAWTs are shown in Table 4. The diagonal lines in the table show several cases with same absolute thicknesses of 3.3%H. Fig. 22 shows the variations of the C_P of VAWTs with two type struts relative to that of VAWTs without struts. It is observed that:

- The power coefficients of the VAWTs with olivary struts are better than those of the NACA airfoil in all cases. Comparing the $C_{P\text{-}Total}$ and the $C_{P\text{-}Blade}$ for both profiles, the olivary struts not only have less profile drag than the NACA airfoil, but also less induced drag. Compared to the blades without struts, for the eight cases in Table 4, the $C_{P\text{-}Total}$ of the turbines with NACA struts are reduced by an average of 39.4%, while the turbines with olivary struts are reduced by a averaged of 29.2%. Thus, the drag of the olivary strut is reduced by 25.8% relative to the NACA strut.
- The olivary struts with longer chord than the blade chord has less drag. As seen in Fig. 22, the power reductions of NACA airfoil and olivary struts are close when c_S<1.00c_B. When c_S⩾1.00c_B, the drag of olivary strut can be reduced significantly. When c_S=1.50c_B, the total C_P of the olivary strut VAWT is reduced by 22.4% compared to the blades without struts. Although the C_P still has significant reduction, it is superior to most struts and even the baseline VAWT with the thin flat strut as seen Fig. 15. What's more, the cross-sectional area of the olivary strut is 7 times larger than that of the flat strut. This indicates that the olivary

struts can provide higher strength while keeping small drag characteristics.

Table 4. Comparison of power coefficients of NACA airfoils and the olivary profiles for different chords and thicknesses corresponding to the left-bottom part of **Table 2**. The upper half of this table is the total power coefficient of the VAWT (including the struts and the tower). The bottom half is the power coefficient only produced by the blades. The numbers colored by red and blue are the NACA and olivary profiles with the same absolute thickness, respectively.

C_{P_Total}	$c_S=0.50c_B$	$c_S=0.75c_B$	$c_S=1.00c_B$	$c_S=1.50c_B$	
$A_S=0.50A_B$	**0.1819**	0.1774			NACA
	0.1907	0.1998			Olivary
$A_S=0.75A_B$		**0.1473**	0.1291		NACA
		0.1700	0.2147		Olivary
$A_S=1.00A_B$		0.0973	**0.0848**		NACA
		0.1192	**0.1690**		Olivary
$A_S=1.50A_B$		-0.0350		**0.1391**	NACA
		-0.0014		**0.2185**	Olivary
C_{P_Blades}	$c_S=0.50c_B$	$c_S=0.75c_B$	$c_S=1.00c_B$	$c_S=1.50c_B$	
$A_S=0.50A_B$	**0.2145**	0.2066			NACA
	0.2252	0.2226			Olivary
$A_S=0.75A_B$		**0.1909**	0.1734		NACA
		0.2028	0.2267		Olivary
$A_S=1.00A_B$		0.1584	**0.1446**		NACA
		0.1690	**0.2013**		Olivary
$A_S=1.50A_B$		0.0893		**0.1860**	NACA
		0.1114		**0.2378**	Olivary

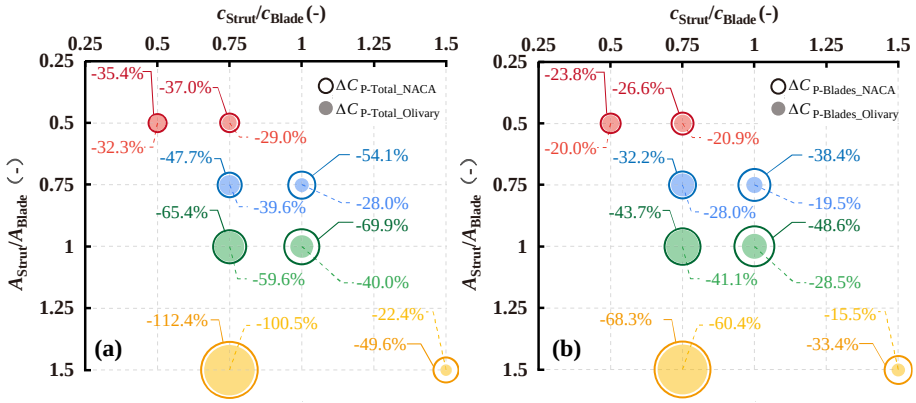

Fig. 22. Relative variations in C_P for VAWTs with and without struts, where $\Delta C_P = (C_{P\text{-}WithStruts} - C_{P\text{-}WithoutStruts})/C_{P\text{-}WithoutStruts}$. The hollow circles represent C_P of VAWTs with NACA airfoil struts. The solid circles represent C_P of VAWTs with olivary profiles. The labels represent relative variation values. (a) The total power coefficients of VAWTs. (b) The power coefficients only from blades.

The C_Q curves of blades installed these two strut profiles and their variation along the spanwise direction are illustrated in Fig. 23. It shows that the induced drag of the olivary strut is smaller (higher C_Q than the NACA airfoil strut). The torque improvement mostly occurs in the upwind region at $60° < \theta < 180°$ and in the downwind region at $240° < \theta < 300°$. When $c_S < 1.00c_B$, the torque improvement of the blade with olivary strut blade only occurs in a small part of the blade and is not significant. When $c_S \geqslant 1.00c_B$, the C_Q of the olivary strut blade is significantly increased up to 0.23.

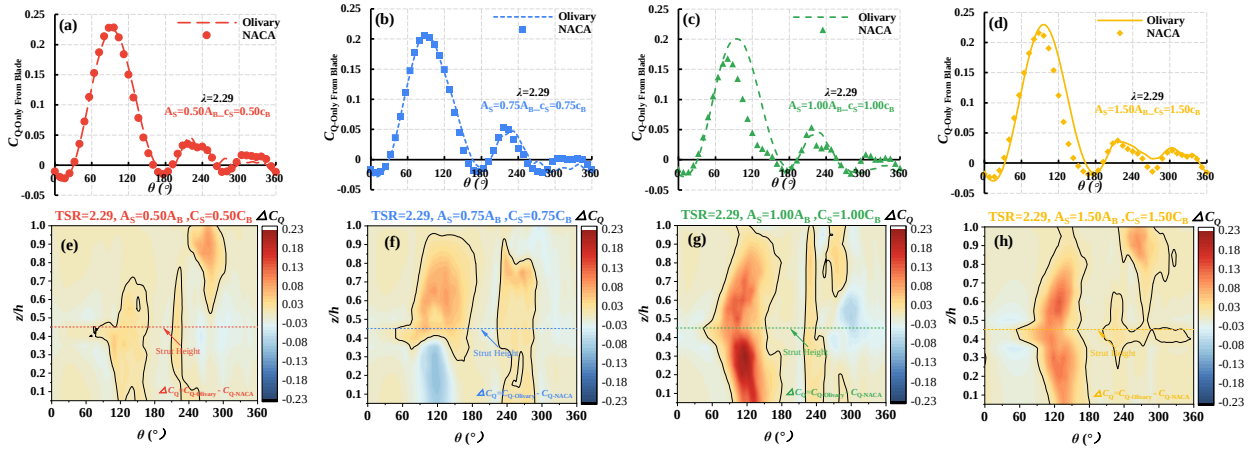

Fig. 23. Comparison of C_Q (only from blades) between the NACA and olivary struts with same absolutely thicknesses of T_{Strut}=3.3% H_{Blade}. (a)~(d) C_Q of the single blade. Different color of these figures corresponding to **Table 2**. (e)~(h) Difference of blade torque coefficients (ΔC_Q) between the NACA and olivary strut along the blade spanwise direction.

(ii) Fluid Field Characteristics

The effects of two types of strut profiles, the NACA airfoil and the olivary, with different chords but the same absolute thickness on the flow characteristics is illustrated in Fig. 24. It shows that in sub-figure (a), the limited streamlines are stagnant at the blade leading edge, which is caused by the large leading edge radius of the NACA airfoil. For the olivary profile in sub-figure (e), the smaller leading edge radius reduces the separation and contributes to mitigate the interference between the strut and the blade. This mitigation effect of the olivary strut is more pronounced when c_S=0.75c_B and c_S=1.00c_B. There is better attached flow in the upper part of the olivary strut blade and the scale of vortex is significantly reduced.

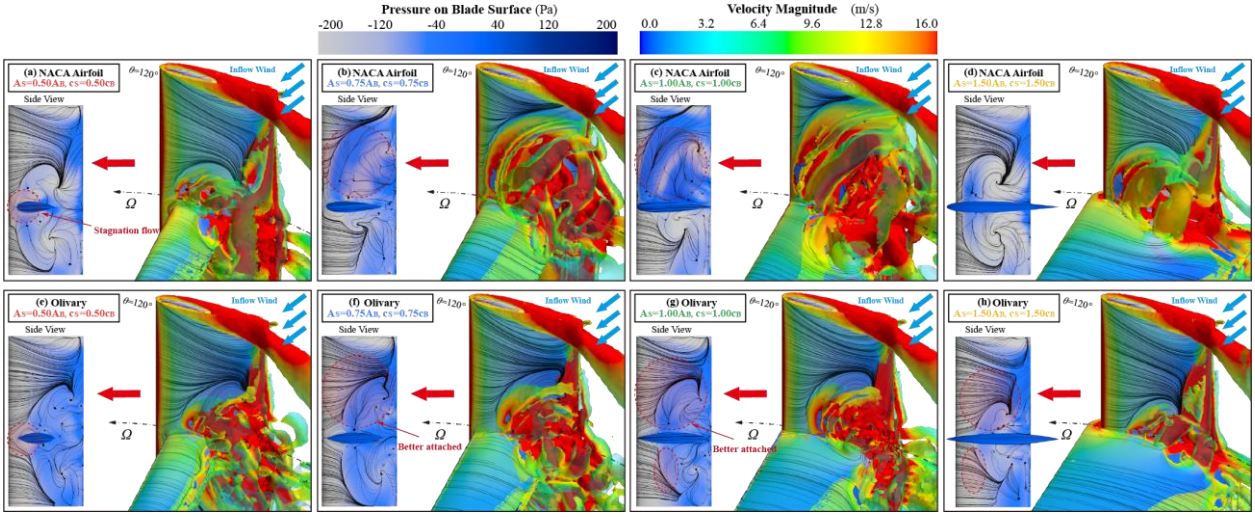

Fig. 24 Comparison of flow characteristics between the VAWTs with different strut profiles. All profiles have the same absolutely thicknesses of T_{Strut}=3.3% H_{Blade} (a)~(d) The NACA airfoil struts. (e)~(h) The olivary struts.

3.3. Influences of Strut Connecting Positions

This section shows the effects of the strut connecting positions, discussed in two aspects: the spanwise position and the chordwise position.

3.3.1. Effects of Spanwise Positions

(i) Aerodynamic Performance

The structural analysis by Mojtaba et al.[40] suggested that the strut should preferably be installed at 0.2H from the blade tip, while the experimental VAWT strut referenced in this paper are at 0.3H. Therefore, the effect of these two spanwise connecting positions is investigated. The variations of the VAWT power coefficients are shown in Fig. 25. Both the NACA airfoil and the olivary profiles are analyzed.

It is observed that the spanwise connecting position closed to the blade tip is beneficial to increase the C_P of

the NACA airfoil strut VAWT, but the effect on the olivary strut VAWT is negligible. In addition, as seen from the difference between C_{P_Blade} and C_{P_Total} in Fig. 25, the variation of the strut spanwise connecting position primarily affects the induced drag, while it has less effect on the profile drag.

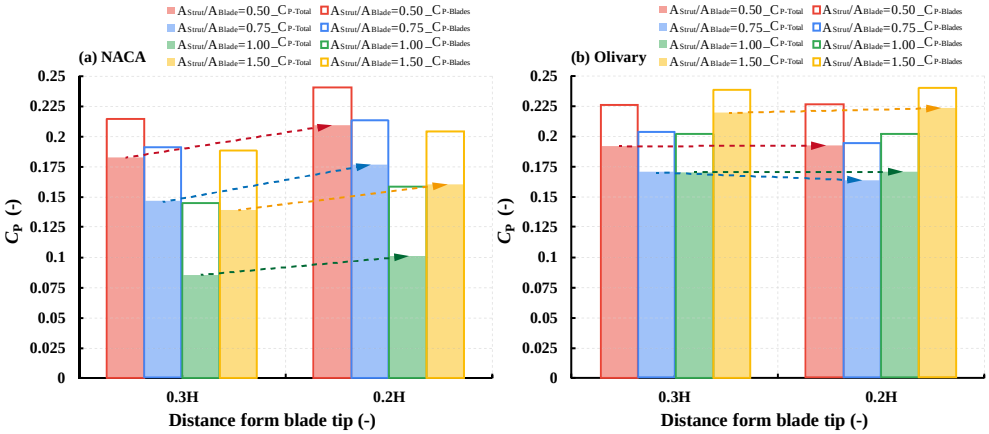

Fig. 25 The power coefficients of VAWTs with different strut spanwise connecting positions. The solid histograms represent the total C_P. The hollow histograms represent the C_P only form blades. (a) The struts use NACA airfoil profiles. (b) The struts use olivary profiles.

(ii) Fluid Field Characteristics

The flow characteristics of the different chord struts installed at 0.2H are shown in Fig. 26. Comparing with the cases of 0.3H struts in Fig. 24, the spanwise connecting position at 0.2H facilitates the attachment of air in the region below the struts, especially for the NACA airfoil struts with c_S<1.00c_B. This is because the large-scale interference generated at the NACA airfoil strut connection overlaps with the spanwise flow induced by the tip loss effects, thus indirectly minimizing the interference below the strut. For the olivary struts, they are insensitive to the variations in spanwise position because their interference with the blades is inherently insignificant.

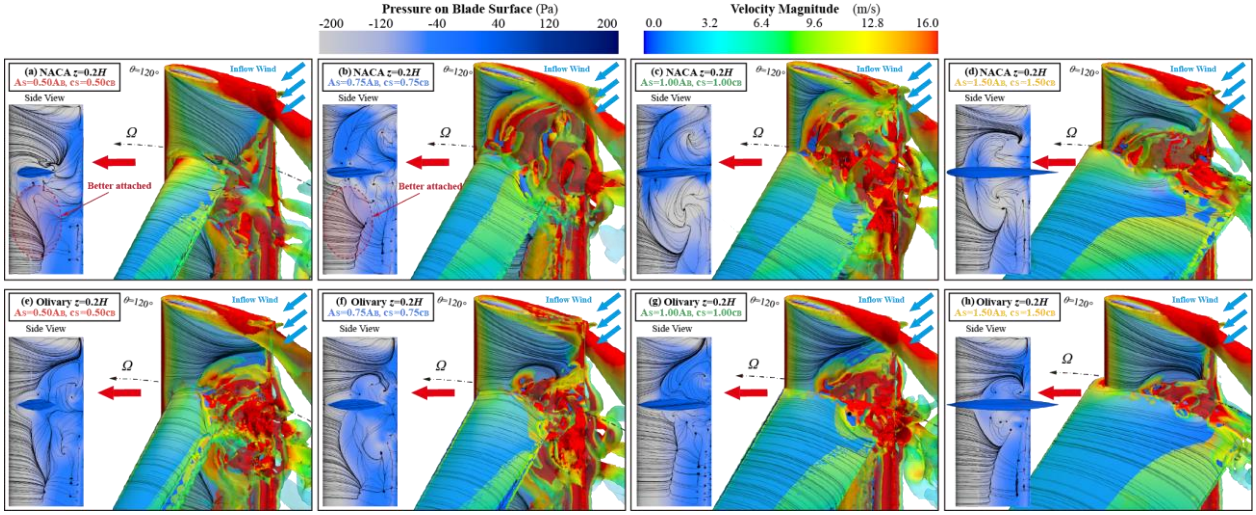

Fig. 26 Flow characteristics of the VAWTs with different profiles of struts installed at z=0.2H. All profiles have the same absolutely thicknesses of T_{Strut}=3.3% H_{Blade} (a)~(d) The NACA airfoil struts. (e)~(h) The olivary struts.

3.3.2. Effects of Chordwise Positions

(i) Aerodynamic Performance

The chordwise connecting positions has not been discussed in past studies when the strut chord is smaller than the blade chord. Therefore, several VAWTs with different strut chordwise connecting positions were established. Fig. 27 shows the power coefficients of these VAWTs.

The C_P are classified by the parameter d_{LE} firstly, as shown in Fig. 27 (a). However, it is difficult to find a general rule for the influence of the strut chordwise position on the aerodynamic performance. In particular, when the strut is changed to olivary profile, there is a remarkable difference with the NACA airfoil strut in the same positions. This raises an issue that why the same area, chord, maximum thickness (either relative or absolute) and

connecting position of the olivary and NACA airfoil struts result in a significant reduction of induced drag for the former.

Observing these two profiles, it is noted that in addition to the difference in leading edge radius, another notable difference is the location of the maximum thickness. Therefore, another parameter d_{MTP}, representing the relative distance between the strut MTP and the blade AC is used to identify the different chordwise positions, as displayed in Fig. 27 (b). Two rules are observed here:

- The aerodynamic efficiency of the VAWT is minimized when the strut MTP coincides with the blade AC (d_{MTP}=0c), as shown by the red dashed line in Fig. 27 (b). This phenomenon is remarkable for the blade with NACA and olivary struts, but not for the baseline flat strut (black histogram). This is explainable because the flat strut does not have a maximum thickness. The C_P of the baseline flat strut VAWT improves with increasing distance from the blade leading edge.
- The aerodynamic performance of all VAWTs is significantly improved when the trailing edge of the strut coincide with the trailing edge of the blade, which is the farthest position of each strut from the blade AC, as illustrated by the marked pentagrams in Fig. 27 (b).

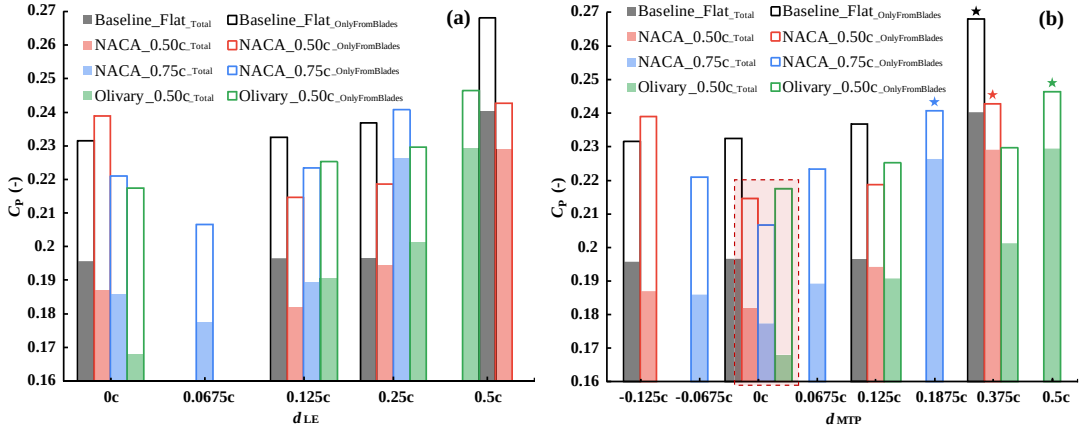

Fig. 27. The power coefficients of VAWTs with different strut chordwise connecting positions. The solid histograms represent the total C_P and the hollow histograms represent C_P only form blades. (a) Claffied by d_{LE}. (b) Claffied by d_{MTP}. The cases with red dotted line and pentagrams are the worst and the best performance respectively.

(ii) Fluid Field Characteristics

The flow characteristics of each strut at different chordwise positions are displayed in Fig. 28. Observed together with the aerodynamic performance in Fig. 27:

- For the streamlined strut profiles with thickness variations, either NACA airfoil or olivary shape, when d_{MTP}=0c, the flow state on the blade surfaces is worse compared to the other strut positions, as shown in Fig. 28 (f) and (m). The reason for this phenomenon may be due to the airflow passing over the blade aerodynamic center (also near the blade MTP) is in a more easily separated state. When the blade AC is connected to the strut MTP, the blade surface flow in the separation critical state is interfered by the strut to the greatest extent. But this speculation needs more evidence to confirm.
- For all struts with different profiles, the closer to the trailing edge, the less influence on the blade surface flow. Taking the baseline flat strut as an example, Fig. 28 (d) shows that the interference of the strut on the blade is slight, even similar to the case without the strut. Comparing with Fig. 18 (b) at θ=90°, it is observed that the surface flow near the trailing edge of the blade without strut will be separated by the spanwise flow due to the tip loss effect. Therefore, installing the strut at the trailing edge position will minimize its influence on the blade. However, this connecting position will cause the aerodynamic forces to generate a pitching moment and induce local stress concentrations at the connection, which is unacceptable for large-scale VAWTs.

In summary, considering the influence of the strut connecting position on the aerodynamic and structural

performance, d_{MTP}=0.125c is a relative better choice.

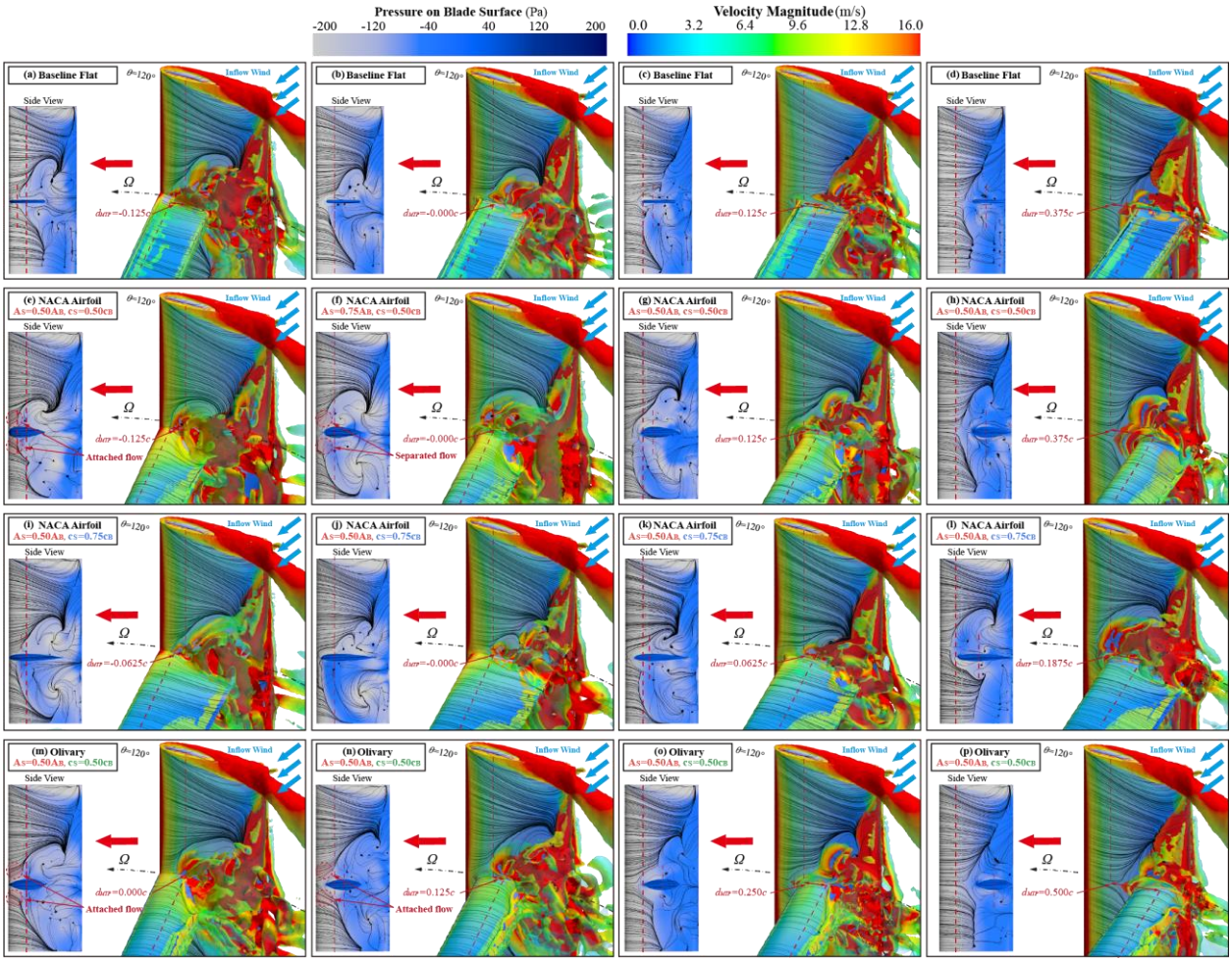

Fig. 28. Flow characteristics of VAWTs for different strut spanwise connecting positions. The red dashed lines are used to indicate the blade AC and the strut MTP. The baseline flat strut is identified with the 0.25c_S since it has no maximum thickness. (a)~(d) The baseline flat struts. (e)~(h) The NACA airfoil struts with c_S=0.50c_B. (i)~(l) The NACA airfoil struts with c_S=0.75c_B. (m)~(p) The olivary struts with c_S=0.50c_B.

3.4. Influences of Strut Connecting Angle

Inclining struts at an angle to lower the center of gravity of the tower is commonly used for large-scale VAWTs. Although Hand et al.[24] suggested a horizontal installed strut to reduce its bending moment, the influence of the inclined strut on the aerodynamic performance is still lacking and worth discussed. Therefore, based on the different strut sizes and profiles, the effect of the inclined strut is investigated in this section.

(i) Aerodynamic Performance

The effect of the inclined strut on the VAWT power coefficients is displayed in Fig. 29. It shows that the drag characteristics of the inclined strut are related to the strut cross-sectional profiles. For the NACA airfoil struts, the inclination is beneficial to improve the efficiency. However, for the olivary profiles, the inclined strut slightly reduces the aerodynamic performance. In addition, compared to the horizontal strut, the inclined NACA airfoil strut reduces both the induced drag and the profile drag, but the inclined olivary strut has insignificant variations in the profile drag. This difference may be due to the fact that the aerodynamic component force of the inclined NACA airfoil strut are able to provide some positive torque[56], while the olivary strut fails to provide lift force due to its special shape.

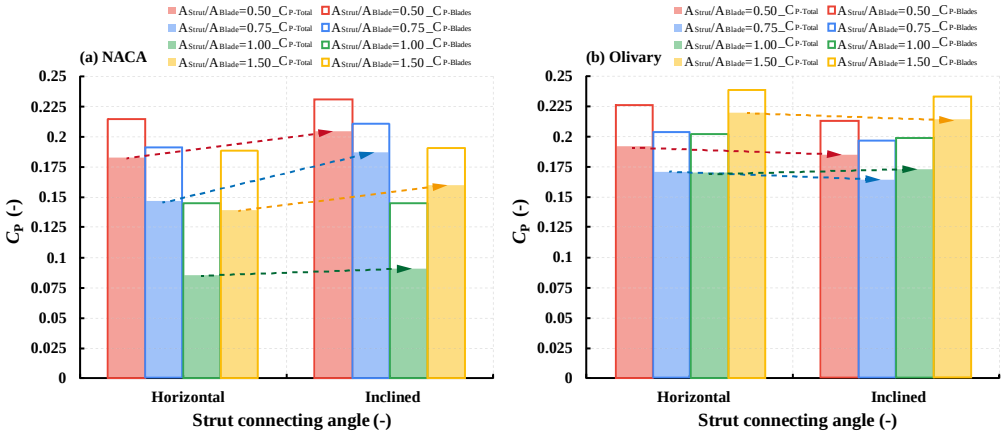

Fig. 29. The power coefficients of VAWTs with different strut connecting angles. The solid histograms represent the total C_P. The hollow histograms represent the C_P only form blades. (a) The struts use NACA airfoil profiles. (a) The struts use olivary profiles.

(ii) Fluid Field Characteristics

The flow characteristics of the VAWTs with horizontal and inclined struts are illustrated in Fig. 30. For the NACA airfoil struts, the inclined installation significantly reduces the vortex scale above the strut, thus improving the flow separation in this region, as shown by the dashed red circles in Fig. 30 (e)~(h). However, the inclined NACA airfoil strut compresses the space below the strut, leading to an increase in separation. These flow characteristics correspond to the variation in aerodynamic performance in Fig. 29. For the olivary struts, the inclined struts have little effect on the blade surface flow, except for the case c_S=1.00c_B. This indicates that the olivary profile is not sensitive to the connecting angle in most cases.

Therefore, if only high aerodynamic efficiency is desired, the inclined VAWT struts may be a good choice, especially for small-scale turbines. However, considering the issue of bending stresses exacerbated by the inclined strut as stated by Hand et al.[24], horizontally installed olivary struts may be more suitable for large-scale VAWTs.

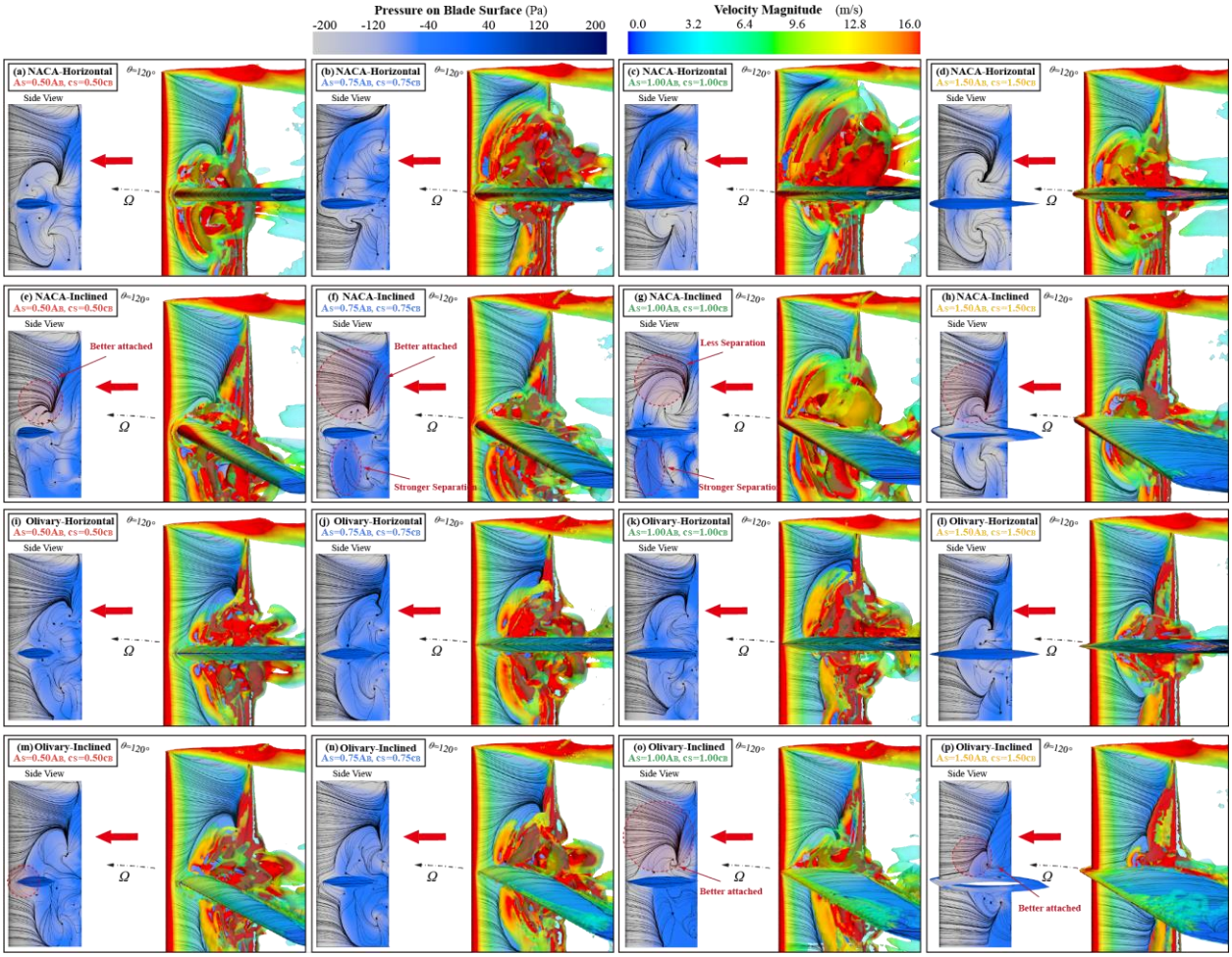

Fig. 30. Flow characteristics of VAWTs for horizontal and inclined struts. (a)~(d) The horizontal NACA airfoil struts. (e)~(h) The inclined NACA airfoil struts. (i)~(l) The horizontal olivary struts. (m)~(p) The inclined olivary struts.

3.5. Influences of Strut-Blade Connecting Fairing

The effect of VAWT strut-blade connecting fairing on aerodynamic performance has not been discussed yet. Consequently, the fairings for struts with different chords and profiles are established.

(i) Aerodynamic Performance

The aerodynamic performance of the VAWT with the NACA airfoil struts adding fairings is shown in Fig. 31 (a). It is observed that the effect of fairing is highly dependent on the strut chord. For cases of $c_S<1.00c_B$ (red and blue histograms), the fairing has a negative effect. The larger the fairing radius, the more significant the blade performance decrease. However, for cases of $c_S\geq1.00c_B$ (green and yellow histograms), the addition of the fairing improves the VAWT efficiency, and the improvement is more obvious for larger radius, especially for $c_S=1.00c_B$.

In addition, to verify whether the fairing effect is affected by the cross-sectional profile, the olivary struts with 0.12c radius are calculated, as shown in Fig. 31 (b). It is observed that the olivary struts also follow the above rule, i.e., the fairing has a positive effect if $c_S\geq1.00c_B$. But the improvement of the olivary strut fairing is not as pronounced as that of the NACA airfoil strut.

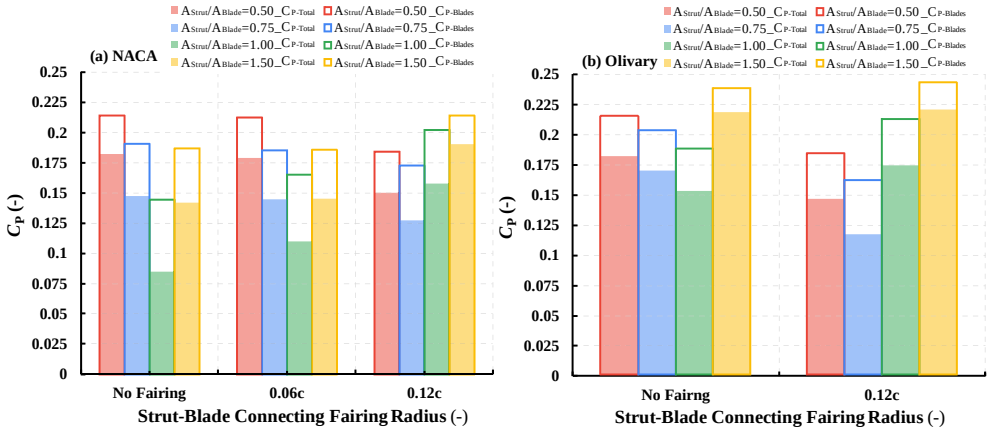

Fig. 31. The power coefficients of VAWTs with different strut-blade connecting fairings. The solid histograms represent the total C_P. The hollow histograms represent the C_P only form blades. (a) The struts use NACA airfoil profiles. (a) The struts use olivary profiles. Only the 0.12c fairing radius are calculated for the olivary struts here.

(ii) Fluid Field Characteristics

The flow characteristics of NACA and olivary struts with 0.12c fairings for different chords are illustrated in Fig. 32. Comparing with the VAWT struts without fairings in Fig. 24, it shows that the fairing exacerbates the separation scale at the leading edge of the connection when $c_S<1.00c_B$, as illustrated by the red dashed lines in (a)~(b) and (e)~(f), which in turn affects the blade surface flow and leads to a reduction in blade torque. For cases of $c_S \geqslant 1.00c_B$, the fairing significantly improves the interference of the strut on the blade surface. In particular, when $c_S=1.00c_B$, the large-scale separation in the blade leading edge region above the NACA airfoil strut is mitigated and replaced by relatively better attached flow.

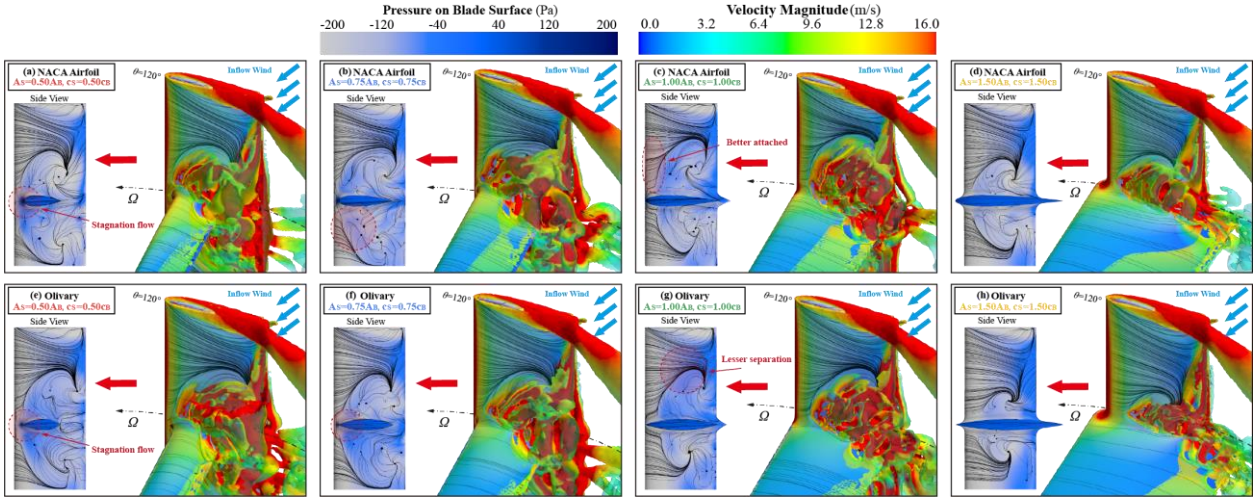

Fig. 32. Flow characteristics of VAWTs with strut-blade connecting fairings radius 0.12c. (a)~(d) The NACA airfoil struts of different chords. (e)~(h) The olivary struts of different chords.

3.6. Summary of Strut Parameters

In summary of the above analysis, Table 5 gives the recommended values for the straight-blade VAWT strut design parameters. These parameters are beneficial for minimizing the influence of the strut on the aerodynamic performance, as well as for the structural strength design requirements of the VAWT struts.

Table 5 Recommended parameter values of straight-bladed VAWT strut.

Parameter	Recommended Value
Cross section	Olivary
Strut chord length	1.5c
Spanwise position	0.2H (From blade tip)
Chordwise posintion	d_{MTP}=0.125c (If $c_S<c_B$)
Connecting angle ξ	ξ=0° (For large tuebine)
Fairing radius	0.12c (When $c_S \geq c_B$)

4. Conclusions

In this paper, the struts of the straight-bladed VAWT are investigated to explore the suitable design parameters that minimize the influence on the VAWT aerodynamic performance. Thirty types of strut profiles including a novel olivary profile with different chord lengths, thicknesses and areas are parametrical modeled based on the equal cross-sectional area principle for the basic supporting strength requirements. VAWTs with these struts are simulated using the accuracy validated CFD model. Then the strut connecting parameters, including the spanwise and chordwise positions, connecting angle, and connecting fairing are analyzed. Some primary conclusions are as following:

(1) The profile and induce drags of the strut substantially reduce the VAWT efficiency. For the strut profile drag related to the characteristic of the cross-sectional shape itself, it is more significant at the azimuth angles where the relative wind speed is stronger ($270^\circ<\theta<390^\circ$). For the induced drag, which is caused by the strut interfering with the blade surface, the interference spreads over the entire blade surface in the spanwise direction, even for the thinnest baseline flat strut. In addition, the induced drag is concentrated on the suction side of the VAWT blade and is most significant in the upwind region ($60^\circ<\theta<180^\circ$). In the downwind region, the induced drag is primarily caused by the wake generated by the struts.

(2) The analysis of VAWT performance for different strut chord lengths, thicknesses and areas shows a general linear relationship between the struts drag characteristics and their absolute thicknesses (a dimensionless parameter based on the blade height). The higher the absolute thickness, the higher the strut drag, and the lower the VAWT performance. On the other hand, for the struts with same cross-sectional area, the larger the chord length (corresponding to a smaller relative thickness) the lower the drag. However, attention should be paid to avoid equal chord lengths for struts and blades, as this will generate the largest vortex scale at the strut-blade connection, resulting in the most severe degradation of blade performance. The strut chord longer than the blade chord is a good choice, which can minimize the vortex scale generated at the connection and reduce the spanwise flow by acting as an endplate.

(3) The olivary profile proposed specifically for VAWT strut has less profile drag and induced drag than the NACA airfoil strut of the same size. Considering the variation of $C_{\text{P-Total}}$ of VAWT, the drag of olivary strut is reduced by 25.8% compared to the NACA strut. Besides, this olivary strut can keep similar drag characteristics with a cross-sectional area 7 times larger than that of the baseline flat strut, which is beneficial for designing a strut with higher structural strength. The flow characteristics analysis shows that the smaller leading edge radius of the olivary profile and the more backward position of the maximum thickness contributes to reduce the interference of the strut with the blade surface flow.

(4) Variations in both the spanwise and chordwise connecting positions affect the VAWT aerodynamic performance. For the spanwise position, the NACA airfoil strut will slightly improve the VAWT efficiency due to the overlap of interfered vortex and blade tip loss effects when the strut is close to the blade tip ($0.2H$). However, the olivary strut is not sensitive to the variation of spanwise position. For the chordwise positions (when $c_S<1.00c_B$), the maximum thickness position of the strut should be avoided to coincide with the blade aerodynamic center. This is because such coincidence leads to the most significant degradation of aerodynamic performance. This holds true for both NACA and olivary struts.

(5) The inclined strut slightly improves the aerodynamic performance of the VAWT with NACA airfoil struts but has a negligible effect on the VAWT with olivary struts. This is because the inclined NACA airfoil strut reduces the vortex scale in the region above the strut and generate some positive torque by itself at the same time. Based on the analysis, it is concluded that an inclined strut is a good choice for small VAWTs with low structural demands. But for large-scale VAWTs, the horizontal installed olivary strut is more recommended to reduce the bending stress inside the strut.

(6) The strut-blade connecting fairing is more suitable for the case of $c_S\geq1.00c_B$, which is valid for both NACA

and olivary struts. Flow analysis shows that the fairing expands the vortex scale at the connection leading edge, resulting in performance degradation when $c_S<1.00c_B$. The opposite is true for the case of $c_S\geq1.00c_B$.

5. Future Work

This paper focuses on the influence of strut design parameters on the aerodynamic performance of the straight-bladed VAWT. Some further works may be studied in the future:

(1) A small VAWT with low aspect ratio is use in this paper because it is convenient to verify with the experimental wind turbine. Although the dimensionless parametric design of the strut scale has been carried out, the effects of some strut parameters related to the spanwise direction, such as the thickness and the spanwise connecting position, still require validation on a high aspect ratio VAWT.

(2) In this paper, struts with constant cross section along the radius direction of the VAWT are employed. However, struts with variable chord length and profile are commonly used in practical applications, especially for large-scale VAWTs. The drag characteristics of variable cross-section struts with different parameters needs to be further confirmed.

(3) Experiments should be conducted in the future to confirm the characteristics of the olivary profile and the strut connecting parameters discussed in this paper.

Acknowledgments

The authors would like to acknowledge the support of National Natural Science Foundation of China (grand No. 52106262, No. 52006148, and No. 51976131). Besides, special thanks to researcher Hand et al[24]. for the work of VAWT that inspired this study.

Reference

[1] Simon-Philippe Breton, Geir Moe. Status, plans and technologies for offshore wind turbines in Europe and North America [J]. Renewable Energy, 2009, 34(3): 646-654.

[2] P. Veers, K. Dykes, E. Lantz, S. Barth, C. L. Bottasso, O. Carlson, A. Clifton, J. Green, P. Green, H. Holttinen, D. Laird, V. Lehtomaki, J. K. Lundquist, J. Manwell, M. Marquis, C. Meneveau, P. Moriarty, X. Munduate, M. Muskulus, J. Naughton, L. Pao, J. Paquette, J. Peinke, A. Robertson, J. Sanz Rodrigo, A. M. Sempreviva, J. C. Smith, A. Tuohy, R. Wiser. Grand challenges in the science of wind energy [J]. Science, 2019, 366(6464): 1-9.

[3] T Composites, Warren, Cost study for large wind turbine blades: WindPACT blade system design studies.[R]. Sandia National Laboratories, 2003.

[4] H. Arabian-Hoseynabadi, H. Oraee, P. J. Tavner. Failure Modes and Effects Analysis (FMEA) for wind turbines [J]. International Journal of Electrical Power & Energy Systems, 2010, 32(7): 817-824.

[5] G. Sieros, P. Chaviaropoulos, J. D. Sørensen, B. H. Bulder, P. Jamieson. Upscaling wind turbines: theoretical and practical aspects and their impact on the cost of energy [J]. Wind Energy, 2012, 15(1): 3-17.

[6] Willy Tjiu, Tjukup Marnoto, Sohif Mat, Mohd Hafidz Ruslan, Kamaruzzaman Sopian. Darrieus vertical axis wind turbine for power generation I: Assessment of Darrieus VAWT configurations [J]. Renewable Energy, 2015, 75: 50-67.

[7] Willy Tjiu, Tjukup Marnoto, Sohif Mat, Mohd Hafidz Ruslan, Kamaruzzaman Sopian. Darrieus vertical axis wind turbine for power generation II: Challenges in HAWT and the opportunity of multi-megawatt Darrieus VAWT development [J]. Renewable Energy, 2015, 75: 560-571.

[8] Michael Borg, Maurizio Collu, Athanasios Kolios. Offshore floating vertical axis wind turbines, dynamics modelling state of the art. Part II: Mooring line and structural dynamics [J]. Renewable and Sustainable Energy Reviews, 2014, 39: 1226-1234.

[9] Michael Borg, Maurizio Collu. Offshore floating vertical axis wind turbines, dynamics modelling state of the art. Part III: Hydrodynamics and coupled modelling approaches [J]. Renewable and Sustainable Energy Reviews, 2015, 46: 296-310.

[10] Michael Borg, Andrew Shires, Maurizio Collu. Offshore floating vertical axis wind turbines, dynamics modelling state of the art. part I: Aerodynamics [J]. Renewable and Sustainable Energy Reviews, 2014, 39: 1214-1225.

[11] Sutherland H J Ashwill T D, Berg D E, A retrospective of VAWT technology[R]. Sandia National Laboratories, 2012.

[12] Weipao Miao, Qingsong Liu, Zifei Xu, Minnan Yue, Chun Li, Wanfu Zhang. A comprehensive analysis of blade

tip for vertical axis wind turbine: Aerodynamics and the tip loss effect [J]. Energy Conversion and Management, 2022, 253: 115140.
[13] Tian-tian Zhang, Mohamed Elsakka, Wei Huang, Zhen-guo Wang, Derek B. Ingham, Lin Ma, Mohamed Pourkashanian. Winglet design for vertical axis wind turbines based on a design of experiment and CFD approach [J]. Energy Conversion and Management, 2019, 195: 712-726.
[14] M. Elkhoury, T. Kiwata, E. Aoun. Experimental and numerical investigation of a three-dimensional vertical-axis wind turbine with variable-pitch [J]. Journal of Wind Engineering and Industrial Aerodynamics, 2015, 139: 111-123.
[15] Willmer A. Wind tunnel tests on a 3m diameter musgrove windmill [J]. Int J Ambient Energy, 1980, 1(1): 21-27.
[16] Longhuan Du, Grant Ingram, Robert G. Dominy. Experimental study of the effects of turbine solidity, blade profile, pitch angle, surface roughness, and aspect ratio on the H‐Darrieus wind turbine self‐starting and overall performance [J]. Energy Science & Engineering, 2019, 7(6): 2421-2436.
[17] Stefania Zanforlin, Stefano Deluca. Effects of the Reynolds number and the tip losses on the optimal aspect ratio of straight-bladed Vertical Axis Wind Turbines [J]. Energy, 2018, 148: 179-195.
[18] Claessens MC. The design and testing of airfoils for application in small vertical axis wind turbines: aerospace engineering[D]. Delft University of Technology, 2006
[19] Mojtaba Tahani, Narek Babayan, Seyedmajid Mehrnia, Mehran Shadmehri. A novel heuristic method for optimization of straight blade vertical axis wind turbine [J]. Energy Conversion and Management, 2016, 127: 461-476.
[20] Islam M, Ting D, Fartaj A. Desirable airfoil features for smaller-capacity straight-bladed VAWT [J]. Wind Energy, 2007, 31(3): 165-196.
[21] S. Brusca, R. Lanzafame, M. Messina. Design of a vertical-axis wind turbine: how the aspect ratio affects the turbine's performance [J]. International Journal of Energy and Environmental Engineering, 2014, 5(4): 333-340.
[22] Abdolrahim Rezaeiha, Ivo Kalkman, Hamid Montazeri, Bert Blocken. Effect of the shaft on the aerodynamic performance of urban vertical axis wind turbines [J]. Energy Conversion and Management, 2017, 149: 616-630.
[23] Aya Aihara, Victor Mendoza, Anders Goude, Hans Bernhoff. A numerical study of strut and tower influence on the performance of vertical axis wind turbines using computational fluid dynamics simulation [J]. Wind Energy, 2022, : 1-17.
[24] Brian Hand, Ger Kelly, Andrew Cashman. Aerodynamic design and performance parameters of a lift-type vertical axis wind turbine: A comprehensive review [J]. Renewable and Sustainable Energy Reviews, 2021, 139: 110699.
[25] Abdolrahim Rezaeiha, Hamid Montazeri, Bert Blocken. Active flow control for power enhancement of vertical axis wind turbines: Leading-edge slot suction [J]. Energy, 2019, 189: 116131.
[26] Jinjing Sun, Xiaojing Sun, Diangui Huang. Aerodynamics of vertical-axis wind turbine with boundary layer suction – Effects of suction momentum [J]. Energy, 2020, 209: 118446.
[27] Haitian Zhu, Wenxing Hao, Chun Li, Qinwei Ding, Baihui Wu. Application of flow control strategy of blowing, synthetic and plasma jet actuators in vertical axis wind turbines [J]. Aerospace Science and Technology, 2019, 88: 468-480.
[28] Qingsong Liu, Weipao Miao, Qi Ye, Chun Li. Performance assessment of an innovative Gurney flap for straight-bladed vertical axis wind turbine [J]. Renewable Energy, 2022, 185: 1124-1138.
[29] You-Lin Xu, Yi-Xin Peng, Sheng Zhan. Optimal blade pitch function and control device for high-solidity straight-bladed vertical axis wind turbines [J]. Applied Energy, 2019, 242: 1613-1625.
[30] Wenxing Hao, Musa Bashir, Chun Li, Chengda Sun. Flow control for high-solidity vertical axis wind turbine based on adaptive flap [J]. Energy Conversion and Management, 2021, 249: 114845.
[31] Alessandro Bianchini, Francesco Balduzzi, Daniele Di Rosa, Giovanni Ferrara. On the use of Gurney Flaps for the aerodynamic performance augmentation of Darrieus wind turbines [J]. Energy Conversion and Management, 2019, 184: 402-415.
[32] Kok Hoe Wong, Wen Tong Chong, Nazatul Liana Sukiman, Yui-Chuin Shiah, Sin Chew Poh, Kamaruzzaman Sopian, Wei-Cheng Wang. Experimental and simulation investigation into the effects of a flat plate deflector on vertical axis wind turbine [J]. Energy Conversion and Management, 2018, 160: 1019-1125.
[33] Zhenyu Wang, Yuchen Wang, Mei Zhuang. Improvement of the aerodynamic performance of vertical axis wind turbines with leading-edge serrations and helical blades using CFD and Taguchi method [J]. Energy Conversion and Management, 2018, 177: 107-121.
[34] Omar S. Mohamed, Ahmed A. Ibrahim, Ahmed K. Etman, Amr A. Abdelfatah, Ahmed M. R. Elbaz. Numerical investigation of Darrieus wind turbine with slotted airfoil blades [J]. Energy Conversion and Management: X, 2020, 5: 100026.
[35] F. Arpino, M. Scungio, G. Cortellessa. Numerical performance assessment of an innovative Darrieus-style vertical axis wind turbine with auxiliary straight blades [J]. Energy Conversion and Management, 2018, 171: 769-777.
[36] M. Scungio, F. Arpino, V. Focanti, M. Profili, M. Rotondi. Wind tunnel testing of scaled models of a newly

developed Darrieus-style vertical axis wind turbine with auxiliary straight blades [J]. Energy Conversion and Management, 2016, 130: 60-70.
[37] Qingsong Liu, Weipao Miao, Chun Li, Winxing Hao, Haitian Zhu, Yunhe Deng. Effects of trailing-edge movable flap on aerodynamic performance and noise characteristics of VAWT [J]. Energy, 2019, 189: 116271.
[38] Lulu Ni, Weipao Miao, Chun Li, Qingsong Liu. Impacts of Gurney flap and solidity on the aerodynamic performance of vertical axis wind turbines in array configurations [J]. Energy, 2021, 215: 118915.
[39] L. Battisti, A. Brighenti, E. Benini, M. Raciti Castelli. Analysis of Different Blade Architectures on small VAWT Performance[C]//Journal of Physics: Conference Series. 2016,753:062009.
[40] Mojtaba Ahmadi-Baloutaki, Rupp Carriveau, David S. K. Ting. Straight-bladed vertical axis wind turbine rotor design guide based on aerodynamic performance and loading analysis [J]. Proceedings of the Institution of Mechanical Engineers, Part A: Journal of Power and Energy, 2014, 228(7): 742-759.
[41] M. Islam, M.R. Amin, D.S-K Ting, A Fartaj. Performance Analysis of a Smaller-capacity Straight-bladed VAWT with Prospective Airfoils[C]//46th AIAA Aerospace Sciences Meeting and Exhibit, Reno, Nevada, USA. 2008.
[42] Brian Hand, Andrew Cashman. Aerodynamic modeling methods for a large-scale vertical axis wind turbine: A comparative study [J]. Renewable Energy, 2018, 129: 12-31.
[43] Mark H. Worstell. Aerodynamic Performance of the DOE/Sandia 17-m-Diameter Vertical-Axis Wind Turbine [J]. Journal of Energy, 1981, 5(1): 39-42.
[44] Qing'an Li, Takao Maeda, Yasunari Kamada, Junsuke Murata, Kento Shimizu, Tatsuhiko Ogasawara, Alisa Nakai, Takuji Kasuya. Effect of solidity on aerodynamic forces around straight-bladed vertical axis wind turbine by wind tunnel experiments (depending on number of blades) [J]. Renewable Energy, 2016, 96: 928-939.
[45] Aya Aihara, Victor Mendoza, Anders Goude, Hans Bernhoff. Comparison of Three-Dimensional Numerical Methods for Modeling of Strut Effect on the Performance of a Vertical Axis Wind Turbine [J]. Energies, 2022, 15(7): 2361.
[46] Peter Bachant, Martin Wosnik, Budi Gunawan, Vincent S. Neary. Experimental Study of a Reference Model Vertical-Axis Cross-FlowTurbine [J]. PLoS One, 2016, 11(9): 1-20.
[47] Mazharul Islam, M. Ruhul Amin, David S-K. Ting, Amir Fartaj. A NewAirfoil for the Supporting Struts of Smaller-capacity Straight-Bladed VAWT[C]//12th AIAA/ISSMO Multidisciplinary Analysis and Optimization Conference, Victoria, British Columbia Canada. 2008.
[48] Philip Marsh, Dev Ranmuthugala, Irene Penesis, Giles Thomas. Three-dimensional numerical simulations of straight-bladed vertical axis tidal turbines investigating power output, torque ripple and mounting forces [J]. Renewable Energy, 2015, 83: 67-77.
[49] Yutaka Hara, Naoki Horita, Shigeo Yoshida, Hiromichi Akimoto, Takahiro Sumi. Numerical Analysis of Effects of Arms with Different Cross-Sections on Straight-Bladed Vertical Axis Wind Turbine [J]. Energies, 2019, 12(11): 2106.
[50] Mazharul Islam, Amir Fartaj, Rupp Carriveau. Analysis of the Design Parameters Related to a Fixed-Pitch Straight-Bladed Vertical Axis Wind Turbine [J]. Wind Engineering, 2008, 32(5): 491-507.
[51] Thierry Villeneuve, Grégoire Winckelmans, Guy Dumas. Increasing the efficiency of vertical-axis turbines through improved blade support structures [J]. Renewable Energy, 2021, 169: 1386-1401.
[52] M. Saqib Hameed, S. Kamran Afaq. Design and analysis of a straight bladed vertical axis wind turbine blade using analytical and numerical techniques [J]. Ocean Engineering, 2013, 57: 248-255.
[53] John Keithley Difuntorum, Louis Angelo M. Danao. Improving VAWT performance through parametric studies of rotor design configurations using computational fluid dynamics [J]. Proceedings of the Institution of Mechanical Engineers, Part A: Journal of Power and Energy, 2018, 233(4): 489-509.
[54] Alessandro Bianchini, Francesco Balduzzi, Giovanni Ferrara, Lorenzo Ferrari. Influence of the blade-spoke connection point on the aerodynamic perfomance of Darrieus wind turbines[C]//In: Proceedings of the ASME turbo expo 2016, Seoul, South Korea. 2016:1-9.
[55] Pierre Blusseau, Minoo H. Patel. Gyroscopic effects on a large vertical axis wind turbine mounted on a floating structure [J]. Renewable Energy, 2012, 46: 31-42.
[56] Agostino De Marco, Domenico P. Coiro, Domenico Cucco, Fabrizio Nicolosi. A Numerical Study on a Vertical-Axis Wind Turbine with Inclined Arms [J]. International Journal of Aerospace Engineering, 2014, 2014: 1-14.
[57] Brian K. Kirke. Evaluation of Self-Starting Vertical Axis Wind Turbines for Stand-Alone Applications[D]. Griffith University, 1998
[58] H. F. Lam, H. Y. Peng. Study of wake characteristics of a vertical axis wind turbine by two- and three-dimensional computational fluid dynamics simulations [J]. Renewable Energy, 2016, 90: 386-398.
[59] Sighard F. Hoerner, Practical information on aerodynamic drag and hydrodynamic resistance[R]. Fluid dynamic drag. Horner fluid dynamics, CA, 1965.
[60] Denis Pitance, Simon Horb, oanna Kluczewska-Bordier, Alexandre Immas, Frédéric Silver, Experimental validation of pharwen code using data from vertical-axis wind turbines[R]. WindEurope PO, 2016.

[61] Qing'an Li, Takao Maeda, Yasunari Kamada, Junsuke Murata, Toshiaki Kawabata, Kento Shimizu, Tatsuhiko Ogasawara, Alisa Nakai, Takuji Kasuya. Wind tunnel and numerical study of a straight-bladed vertical axis wind turbine in three-dimensional analysis (Part I: For predicting aerodynamic loads and performance) [J]. Energy, 2016, 106: 443-452.
[62] Qing'an Li, Takao Maeda, Yasunari Kamada, Junsuke Murata, Toshiaki Kawabata, Kento Shimizu, Tatsuhiko Ogasawara, Alisa Nakai, Takuji Kasuya. Wind tunnel and numerical study of a straight-bladed Vertical Axis Wind Turbine in three-dimensional analysis (Part II: For predicting flow field and performance) [J]. Energy, 2016, 104: 295-307.
[63] Manwell JF, McGowan JG, Rogers AL. Wind energy explained: Theory, design and application[M]. John Wiley & Sons, 2002
[64] C. L. Ladson, Cuyler W.Jr. Brooks, Development of a computer program to obtain ordinates for NACA 4-digit, 4-digit modified, 5-digit, and 16 series airfoils[R]. No. L-10375, 1975.
[65] Marco Raciti Castelli, Guido Ardizzon, Lorenzo Battisti, Ernesto Benini, Giorgio Pavesi. Modeling Strategy and Numerical Validation For A Darrieus Vertical Axis Micro-Wind Turbine[C]//Proceedings of the ASME 2010 International Mechanical Engineering Congress & Exposition, Canada，British Columbia. 2010.
[66] L. Battisti, G. Persico, V. Dossena, B. Paradiso, M. Raciti Castelli, A. Brighenti, E. Benini. Experimental benchmark data for H-shaped and troposkien VAWT architectures [J]. Renewable Energy, 2018, 125: 425-444.
[67] Ning Ma, Hang Lei, Zhaolong Han, Dai Zhou, Yan Bao, Kai Zhang, Lei Zhou, Caiyong Chen. Airfoil optimization to improve power performance of a high-solidity vertical axis wind turbine at a moderate tip speed ratio [J]. Energy, 2018, 150: 236-252.
[68] P. J. Roache. Quantification of Uncertainty in Computational Fluid Dynamics [J]. Annu Rev Fluid Mech, 1997, 29: 123–160.
[69] S. Zadeh, M. Komeili, M. Paraschivoiu. Mesh convergence study for 2-d straight-blade vertical axis wind turbine simulations and estimation for 3-d simulations [J]. Transactions of the Canadian Society for Mechanical Engineering, 2014, 38(4): 487-503.
[70] Abdolrahim Rezaeiha, Hamid Montazeri, Bert Blocken. Towards accurate CFD simulations of vertical axis wind turbines at different tip speed ratios and solidities: Guidelines for azimuthal increment, domain size and convergence [J]. Energy Conversion and Management, 2018, 156: 301-316.
[71] László Daróczy, Gábor Janiga, Klaus Petrasch, Michael Webner, Dominique Thévenin. Comparative analysis of turbulence models for the aerodynamic simulation of H-Darrieus rotors [J]. Energy, 2015, 90: 680-690.
[72] Abdolrahim Rezaeiha, Hamid Montazeri, Bert Blocken. On the accuracy of turbulence models for CFD simulations of vertical axis wind turbines [J]. Energy, 2019, 180: 838-857.
[73] Abdolrahim Rezaeiha, Hamid Montazeri, Bert Blocken. CFD analysis of dynamic stall on vertical axis wind turbines using Scale-Adaptive Simulation (SAS): Comparison against URANS and hybrid RANS/LES [J]. Energy Conversion and Management, 2019, 196: 1282-1298.
[74] Mikhail L. Shur, Philippe R. Spalart, Mikhail Kh Strelets, Andrey K. Travin. A hybrid RANS-LES approach with delayed-DES and wall-modelled LES capabilities [J]. International Journal of Heat and Fluid Flow, 2008, 29(6): 1638-1649.
[75] Hang Lei, Dai Zhou, Yan Bao, Ye Li, Zhaolong Han. Three-dimensional Improved Delayed Detached Eddy Simulation of a two-bladed vertical axis wind turbine [J]. Energy Conversion and Management, 2017, 133: 235-248.
[76] Jacobs EN, Sherman A, Airfoil section characteristics as affected by variations of the Reynolds number. Tech. rep.[R]. Washington. D.C National Advisory Committee for Aeronautics, 1939.